Per. Mineral. (2000), *69*, 3, 269-310 http://go.to/permin

PERIODICO di MINERALOGIA
established in 1930

An International Journal of
MINERALOGY, CRYSTALLOGRAPHY, GEOCHEMISTRY, ORE DEPOSITS, PETROLOGY, VOLCANOLOGY
and applied topics on *Environment, Archaeometry* and *Cultural Heritage*

Petrology and mineral chemistry of late-Hercynian dykes from NW Corsica (France)

NICOLETTA BURAGLINI[1] and GIANBOSCO TRAVERSA[2]*

[1] Dipartimento di Scienze della Terra, Università di Catania, C.so Italia 55, 95129 Catania, Italy
[2] Dipartimento di Scienze della Terra, Università di Roma "La Sapienza", P.le A. Moro 5, 00185 Roma, Italy

Submitted, July 2000 - Accepted, November 2000

ABSTRACT. — Intense late- to post-collisional dyke magmatism characterizes NW Corsica, starting from the last phases of Hercynian orogeny, intruding prevalently the Carboniferous granitoids and subordinately the rhyolites belonging to the calc-alkaline Lower Permian volcanism. Both acidic and basic dykes are represented, whereas there is an evident gap in the intermediate compositions; lack of crosscutting evidence do not allow us to constrain the timing of emplacement of the various magmatic units. Basic dykes comprise calcalkaline and mildly alkaline litotypes, ranging in composition respectively from basaltic andesite to andesite and from alkali basalt (dolerite) to basaltic-trachyandesite; among the latter, a fractionation link is supported by mass balance calculations. The acidic dykes are mainly composed of metaluminous granitic porphyries and subordinate peraluminous microgranites, both preferentially NE-SW oriented, and by peralkaline aplites. REE and trace elements modeling indicate derivation from a possibly subduction-modified litospheric mantle source for both calcalkaline and mildly alkaline basaltic dykes, together with crustal contamination probably undergone by magmas as they ascend to the surface, as testified by Rb and Pb positive spikes relative to primitive mantle composition. However, higher Nb and Ta contents for mildly alkaline dykes relate them to a less depleted mantle source compared to calcalkaline ones, to be referred to a post-collisional domain predating a true intracontinental rift-related phase. Instead, the calcalkaline dykes were emplaced in a preceding phase still characterized by an orogenic imprint, also shown by peraluminous microgranites. These are probably anatectic melts deriving from a metasedimentary or meta-igneous protolith. Preliminary $^{40}Ar/^{39}Ar$ geochronological data from the biotite and muscovite of a few samples indicate an age around 320 Ma, suggesting that these peraluminous microgranites are related to a magmatic event connected with the Mg-K calcalkaline association dated at 322±12 Ma (Cocherie *et al.*, 1992).

Granitic porphyries and peralkaline aplites show geochemical characters typical of A-type granites and are referred to an anorogenic tectonic setting. Strong petrographic and geochemical similarities with Upper Permian peralkaline granite from Evisa indicate a mantle signature (Bonin, 1978).

* Corresponding author, E-mail:
gianbosco.traversa@uniroma1.it

Moreover, crustal involvement in the genesis of the peralkaline dykes is highlighted by their high Th enrichments.

RIASSUNTO. — Un'intensa attività magmatica filoniana post-collisionale caratterizza la Corsica nord-occidentale a partire dalle ultime fasi dell'Orogenesi Ercinica, interessando soprattutto i granitoidi carboniferi e subordinatamente le rioliti del ciclo vulcanico calcoalcalino del Permiano inferiore. Sono presenti sia filoni acidi che basici, mentre praticamente assenti sono quelli di composizione intermedia. Sul terreno non si osservano situazioni di intersezione reciproca dei filoni di diversa natura, cosicché non è possibile stabilire una sequenza temporale di messa in posto. I filoni basici sono rappresentati da litotipi ad affinità calcoalcalina e moderatamente alcalina, con composizioni che variano rispettivamente da andesiti basaltiche ad andesiti e da basalti alcalini (doleriti) a trachi-andesiti basaltiche; tra questi ultimi prodotti esiste un legame di frazionamento evidenziato dai bilanci di massa. I filoni acidi sono rappresentati da prevalenti porfidi granitici metalluminosi e subordinati microgranitи peralluminosi, che mostrano entrambi una direzione preferenziale d'intrusione NE-SW, e da apliti peralcaline. L'andamento dei patterns degli elementi in traccia e delle REE indica, sia per i filoni calcoalcalini sia per quelli basaltici moderatamente alcalini, derivazione da una sorgente mantellica possibilmente metasomatizzata da un precedente evento subduttivo ed evidenzia anche, sulla base degli arricchimenti in Rb e Pb, una contaminazione crostale cui i magmi sarebbero stati sottoposti durante la loro risalita. Tuttavia, i valori più elevati di Nb e Ta dei filoni basaltici moderatamente alcalini rispetto a quelli calcoalcalini evidenziano una relazione con una sorgente mantellica meno impoverita, in un ambiente geodinamico post-collisionale che anticipa un'autentica fase di rift intracontinentale. I filoni calcoalcalini, invece, si mettono in posto in una fase precedente ancora influenzata dagli eventi orogenici. Anche i microgranitи peralluminosi mostrano impronta orogenica e sono verosimilmente d'origine anatettica, derivati da un originario protolite metasedimentario o metaigneo. Datazioni preliminari eseguite con il metodo $^{40}Ar/^{39}Ar$ su biotite e muscovite di pochi campioni indicano un'età di circa 320 Ma, che ci permette di attribuire a questi microgranitи peralluminosi il significato di un evento magmatico legato all'associazione calcoalcalina magnesio-potassica datata a 322±12 Ma (Cocherie *et al.,* 1992).

I porfidi granitici e le apliti peralcaline mostrano i caratteri tipici dei graniti tipo A riferibili ad un ambiente geodinamico anorogenico. Le marcate affinità petrografiche e geochimiche con i graniti peralcalini di Evisa del Permiano Superiore indicano un'impronta mantellica (Bonin, 1978). Gli elevati arricchimenti in Th testimoniano inoltre un contributo crostale nella genesi dei filoni peralcalini.

KEY WORDS: *NW Corsica, Hercynian orogeny, dyke magmatism, crustal contamination, tectonic setting.*

INTRODUCTION

Numerous dyke swarms crosscut Hercynian plutons and post-orogenic Permian volcanic formations in NW Corsica. Detailed field work and sampling led us to the identification of basic and acidic dykes of different affinities.

In the Balagne region, we recognized a main NE-SW-trending dyke swarm represented by metaluminous granitic porphyries and peraluminous microgranites, together with less widespread mafic dykes of both calc-alkaline and alkaline affinity. Recently, ZEM and U-Pb ages, respectively of 289±3 and 305±2 Ma, have been reported for last ones (Carmignani and Rossi, 2000). Moreover, U/Pb SHRIMP ages of 288±2 and 280±2 Ma, performed on basic dyke rocks of the same area, are in press (Ph. Rossi, pers. comm.). In the Balagne region Fumey-Humbert *et al.* (1986) first recognized an important dyke swarm of calc-alkaline affinity, made up of lithotypes ranging from quarzitic microdiorite to microgranite, the latter prevailing. Comparable mineralogical and geochemical features led the authors to consider these dykes as possible feeder pipes of the Lower Permian calc-alkaline volcanism present in the same area and to date them, on the basis of field evidence, to a period ranging from Middle-Upper Carboniferous to Upper Permian.

Upper Permian alkaline and peralkaline

dykes are another important event of late-Hercynian NW Corsica dyke magmatism. They are mainly represented by rhyolitic sills and ring-dykes, making up the last stage in the evolution of the Mt. Cinto caldera (Cabanis *et al.*, 1990, fig. 1) and subordinate peralkaline linear dykes («paisanites», Quin, 1968) associated with the Evisa and Bonifatto complexes (Bonin, 1988; Egeberg *et al.*, 1993). South of Mt. Cinto we detected aplite and granitic porphyries with peralkaline affinity, together with alkaline doleritic dykes. Sm-Nd age of 258.5±5.8 Ma is reported for doleritic rocks outcropping in the same area (Evisa; Carmignani and Rossi, 2000). Moreover, doleritic dykes have been previously identified by Cabanis *et al.* (1990) in the Porto-Girolata area and by Vellutini (1977) in the Cinto-Scandola area (fig. 1). Their geological setting, crosscutting all previous formations, seems to mark the end of the post-collisional Hercynian magmatic activity. Available ages for these alkaline doleritic dykes are those of van Tellingen *et al.* (1996), who present apatite fission track and K-Ar data for the Aghia-Campana mafic dyke swarm and the granitic host rock (fig. 1). Apatite ages of dolerite range from 21 to 23 Ma; those of granite range from 51 to 203 Ma; K-Ar determinations on whole rock fluctuate between 80 and 140 Ma for dolerite, and are around 40 Ma for granitic contact rocks. We believe that these data indicate re-opening of the system as a result of low-grade metamorphic events after the Upper Permian. Instead, van Tellingen *et al.* (1996) consider these doleritic dykes, which are not present in Eastern Alpine Corsica, as Early Miocene in age and relate them to the rifting and opening of the Gulf of Lion.

The aim of the present paper was the petrographic and geochemical investigation of acidic and basic dykes from NW Corsica, in order to define their relations with Sardinian (Atzori and Traversa, 1986; Vaccaro *et al.*, 1991; Traversa and Vaccaro, 1992; Ronca and Traversa, 1996; Traversa *et al.*, 1997; Ronca *et al.*, 1999) and Corsican (Pasquali and Traversa, 1996; Pasquali, 1998; Simei, 1999) late Hercynian activity and their petrogenesis as possible reference marks for the geodynamic evolution of the area after the last phases of the Hercynian orogeny and before Early Alpine events.

Lack of crosscutting field evidence prevents us from dating the emplacement of the various magmatic units; thus $^{40}Ar/^{39}Ar$ age determinations are forthcoming.

GEOLOGICAL BACK-GROUND AND FIELD DATA

The islands of Corsica and Sardinia host the Corsican-Sardinian Batholith (CSB) which formed during the late- and post-tectonic phases of the Hercynian orogeny between approximately 330 and 280 Ma. The CSB is made up of several multiple intrusions of granitoid plutons and subordinate gabbroic complexes emplaced in upper-middle crustal levels.

The present position of the Sardinian-Corsican microplate is the result of its detachment from the European continental plate and later counterclockwise rotation (Vigliotti and Langenheim, 1995).

The CSB and its metamorphic basement were involved in large-scale late Hercynian dyke magmatism which may mark the transition between an orogenic/post-orogenic setting, characterized by calc-alkaline and peraluminous magmatism, and an anorogenic event, represented by magmatism with alkaline affinity (Atzori and Traversa, 1986; Platevoet and Bonin, 1991; Traversa *et al.*, 1997). The same situation has also been recognized in other sections of the Southern European Hercynian chain, e.g., the Pyrenean Axial Zone (Debon and Zimmermann, 1993) and Middle Iberian Hercynian range (Huertas and Villaseca, 1994).

Pre-batholithic terranes in Corsica are made up of small random outcrops, whereas in Sardinia the metamorphic basement is more extensive.

The magmatic formations making up the CSB belong to different associations displaying various ages and spatial distributions.

– The oldest of these is the Mg-K calc-alkaline association (322±12 Ma by ZEM method, Cocherie *et al.,* 1992), most exclusively present in NW Corsica (Orsini, 1980; see fig. 1). It is characterized by the deepest level of intrusion, most probably related to syn/late-tectonic emplacement. Products range from monzonite to leucomonzogranite, often closely associated with mafic rocks ranging in composition from diorite to syenomonzonite and forming enclaves and even stocks (Menot and Orsini, 1990). On the basis of isotope data, Cocherie *et al.* (1994) suggest mixing between mantle-derived material and a crustal component for the genesis of the mafic rocks; however, the crustal end-member is not the same one that gave rise to the granitoids, which may have derived by FC from a primitive monzodioritic liquid originated by partial melting of a greywacke source (Rossi and Cocherie, 1991). Mafic enclave-bearing granitoids are thus only evidence of magma mingling.

Synkinematic sgranites (Macera *et al.,* 1989), more or less peraluminous and possibly related to this phase, has also been detected in northern Sardinia; their different age (300-305 Ma, Rb-Sr age determinations on minerals and whole rock) and composition compared with the Corsican monzogranites suggest different times of emplacement between the Sardinian and Corsican synkinematic phases.

The NW Corsica Mg-K calcalkaline granitoid intrusions display sub-meridian oriented magmatic structures, which can be observed at all levels, both in mineral orientation and in contacts between different units (Menot and Orsini, 1990).

– The calcalkaline association *s.s.,* the most important magmatic phase in the CSB formation, is characterized by widespread products in both Corsica and Sardinia (Ghezzo and Orsini, 1982, fig. 1). Its emplacement, occurring in a structural framework of uplifting and contemporary crustal extension during post-orogenic phases, is not as deep as that of the Mg-K calc-alkaline association, to the extent that in the external zone of the CSB (SW Sardinia) magmatic intrusions are located in metamorphic terranes of very low grade (Carosi *et al.*, 1992).

The latest age determinations for the Corsican calc-alkaline association indicate 305±12 Ma (ZEM, Rossi *et al.,* 1993), whereas for Sardinia several data have been reported from various complexes all over the island. Average Rb-Sr ages cluster around 310-289 Ma for southern Sardinia (Cocozza *et al.*, 1977; Nicoletti *et al.,* 1982; Secchi *et al.,* 1991) and 297-292 Ma for northern Sardinia (Del Moro *et al.,* 1975).

The intrusions follow a NW-SE regional trend, very clearcut in the Corsican region of Ajaccio-Sartène (Rossi, 1986), which gradually becomes less evident southward (southern-central Sardinia). Relative acidic products are represented by a tonalitic-granodioritic-monzogranitic suite (Menot and Orsini, 1990) together with post-tectonic leucogranite; mafic products are mainly gabbros and diorite up to gabbrotonalite set within mafic-ultramafic complexes (e.g.: Pila Canale and Lévie, Corsica; Punta Falcone and Burcei, Sardinia). Both gabbros and diorite are presumed to be of primary mantle origin (Tommasini and Poli, 1992; Cocherie *et al.,* 1994), whereas differentiation from a mantle-derived basaltic parent magma is suggested for the genesis of gabbrotonalite from the Burcei complex (Brotzu *et al.,* 1993). Mixing processes between mantle- and crust-derived magmas are prevalently advocated for the formation of the tonalitic-granodioritic products (Tommasini and Poli, 1992; Cocherie *et al.,* 1994). Instead, the origin of the more evolved rocks, monzogranite and leucogranite, is controversial. Some authors suggest an origin through partial melting of crustal material (Poli *et al.,* 1989; Cocherie *et al.,* 1994); others support mixing processes considering only leucogranite as typical minimum melt generated by crustal anatexis (Bralia *et al.,* 1981).

– Post-tectonic leucogranite cuts the calc-

alkaline formations, following a NE-SW trend (Marre and Rossi, 1981). In Corsica their age is around 284±20 Ma (ZEM, Rossi *et al.,* 1993); in northern Sardinia Rb-Sr ages of 274±9 Ma were reported by Castorina and Petrini (1989). Their intrusion in the upper crust highlights an extensional tectonic environment which characterizes the Permian period and its associated volcanic activity (Bonin, 1980).

– Post-batholitic calc-alkaline volcanism, the products of which range from andesite to rhyolite (mainly ignimbrite), is well represented in NW Corsica (fig. 1) and in northern and central Sardinia (e.g.: Gallura, Nurra and Barbagia regions). An Autunian age has been attributed on a stratigraphic basis (Vellutini, 1977; Traversa, 1979; Fontana *et al.,* 1982) and by the K-Ar method (267±7 Ma, Edel *et al.,* 1981; Lombardi *et al.,* 1974).

– Upper Permian alkaline-peralkaline vulcano-plutonism is represented mostly in central and northern Corsica, where make up almost 20 ring-dyke complexes (e.g.: Cauro-Bastelica, Evisa, Cinto-Calasima, Capo Rosso, Mt. Cinto, etc.), and subordinately in Sardinia. Rb-Sr whole-rock data on hypersolvus peralkaline granite from the Evisa complex give an age of 246±7 Ma (Bonin *et al.,* 1978). The same lithotypes were dated by the Sm-Nd method (Poitrasson *et al.,* 1998) on various minerals (259±6 Ma) and alkali-feldspar and whole-rock (209±14 Ma): 209±14 Ma may represent a rejuvenated age. Earlier, Maluski (1974, 1976) had made K-Ar and $^{40}Ar/^{39}Ar$ determinations on minerals from the peralkaline granite of the Cauro-Bastelica and Mt. Cinto ring complexes, indicating ages between 280 and 250 Ma; measurements on zircons by the U-Pb method (Maluski and Lancelot, 1976), only for the Cauro-Bastelica peralkaline granite, give an age of 262±13 Ma. Three occurrences have been reported so far for the Sardinian alkaline-peralkaline magmatism. Subsolvus granite ring-dykes are described in Gallura by Bruneton *et al.* (1976); in SE Sardinia rhyolite from Monti Ferru is subsolvus alkaline (Pupin in press; Bonin, pers.comm.) and fayalite-bearing pegmatite is related to the subsolvus Quirra granite (Pani *et al.,* 1997).

As regards late Hercynian dyke magmatism, Traversa (1968, 1969) first detected basic dykes cutting Permian ignimbritic units in northern Sardinia. Later research focused on southern Corsica and northern Sardinia in order to detect possible relative rotation between the two islands (Arthaud and Matte, 1976; Westphal *et al.,* 1976; Vigliotti *et al.,* 1990).

Detailed field and petrological studies initiated by Atzori and Traversa (1986) in Sardinia revealed the abrupt change in dyke direction, from NE-SW in the north to NW-SE in central and southern areas. These studies were followed by intense petrological, geochemical and geochronological investigations, which highlighted at least two different episodes in this magmatic activity. The first episode is represented by calc-alkaline products, whereas the second is mainly basaltic in nature; both are also associated with metaluminous and peraluminous rhyolitic dykes. The calc-alkaline phase was emplaced in two different periods: Carboniferous-Permian boundary (298-289 Ma, Rb-Sr ages) and Lower Permian (around 270 Ma, $^{40}Ar/^{39}Ar$ ages) (Vaccaro *et al.,* 1991; Traversa *et al.,* 1997; Ronca *et al.,* 1999). Recently Atzori et al. (pers. comm.) obtained biotite Rb-Sr ages ranging from 291±3 to 271±3 Ma on a calc-alkaline dyke swarm outcropping in mid-eastern Sardinia and ranging in composition from basaltic andesite to dacite-rhyolite. The basaltic phase is represented by prevailing transitional basalts; alkaline ones are mostly limited to the north (Gallura) and give $^{40}Ar/^{39}Ar$ ages around 230 Ma (Baldelli *et al.,* 1986; Vaccaro *et al.,* 1991).

It is noteworthy that Del Moro *et al.* (1996) obtained a Rb-Sr age of 288±11 Ma for rhyolite in the Autunian volcanic sequence of northern Sardinia, until now considered to be 267±7 Ma (Edel *et al.,*1981). This last circumstance may reset the upper limit of post-batholitic calc-alkaline volcanism in this area. As a consequence, most of the late Hercynian dyke activity regarding at least northern

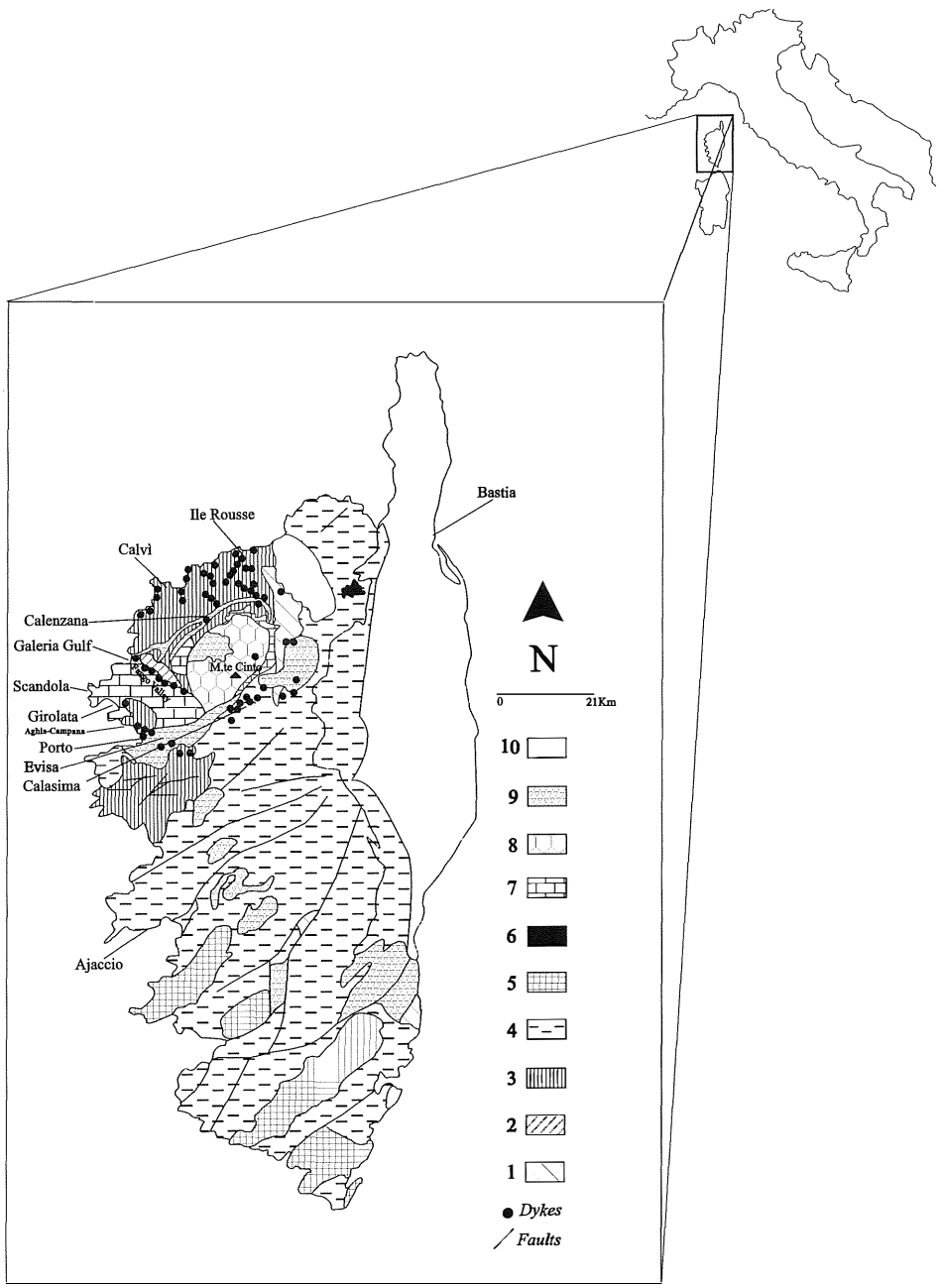

Fig. 1 – Geological sketch map of Corsica (modified after Cocherie *et al.,* 1994) and distribution of sampled dyke rocks. 1 = metamorphic basement; 2 = Paleozoic formations; 3 = granitoids from calc-alkaline Mg-K association; 4 = granodiorite and monzogranite from calc-alkaline association *s.s.;* 5 = leucomonzogranite from calc-alkaline association *s.s.*; 6 = mafic and ultramafic rocks; 7 = Lower Permian calc-alkaline volcanism; 8 = Upper Permian alkaline volcanic rocks; 9 = Upper Permian alkaline plutonic rocks; 10 = Mesozoic formations.

Sardinia would postdate Permian volcanism, except for the 298-289 Ma calc-alkaline phase (Vaccaro *et al.,* 1991).

The late Hercynian dyke magmatism of southern Corsica is similar to that of northern Sardinia, as regards both the geochemical signature and the comparable directions of intrusion (Pasquali and Traversa, 1996; Pasquali, 1998). In southern Corsica two main trends have been recognized in the dyke setting: the main one is NE-SW-oriented, and the second is NS (Pasquali and Traversa, 1996). These trends correspond to those of the same dykes in northern Sardinia, thus further confirming previous geological and paleomagnetic data which highlighted the lack of relative movements between Corsica and Sardinia at the end of the Hercynian orogeny. Moreover, the different orientations displayed by the dykes in southern and central Sardinia compared with those of northern Sardinia and Corsica, together with paleomagnetic data, suggest the possible separation of the Sardinian-Corsican microplate at least in two areas, characterized by different kinematic histories probably more complicated than simple drift and counterclockwise rotation (Pasquali and Traversa, 1996). Also, among the basic dykes of southern Corsica, two large groups of rocks have been recognized. The first is represented by calc-alkaline lithotypes of prevalent basaltic andesite and andesite compositions associated with rare dacite, the second by scarce alkali basalt and by prevalent transitional and tholeiitic lithotypes. A third group is represented by dykes with metaluminous to peraluminous rhyolitic composition (microgranite, quartz porphyry, aplite and micropegmatite) showing no apparent link with less evolved magmas.

The dykes examined in this study come from NW Corsica (fig. 1), i.e, the most northerly section of the CSB. Geologically, this area contains both plutonic complexes belonging to Carboniferous magmatism and products of post-orogenic Permian volcanism. Pre-batholitic metamorphic basement also outcrops to the east.

Most of the dykes, represented by microgranites and granitic porphyries, intrude the porphyritic monzogranite of the Mg-K calcalkaline association in Balagne, the region south of Calvi and Ile Rousse (fig. 1). Prevailing directions are N54E (NE-SW) and N15W, in accordance with data reported by Fumey-Humbert *et al.* (1986) on calc-alkaline dyke swarms from the same area, compositionally ranging from «quartzitic microdiorite» to prevailing microgranite and whose outcropping direction is N60E. Instead, the basic dykes from Balagne show quite disperse orientations. A dense dyke swarm also intrudes the same porphyritic monzogranite near Porto and Evisa; these are basic and basic-intermediate dykes with calc-alkaline and mildly alkaline affinity, preferentially oriented E-W and subordinately N45E and N75W (fig. 2).

Small masses of granitic porphyry with rhyolitic composition were sampled near the Gulf of Galéria (along the Fango river, see fig. 1). They intrude both Lower Carboniferous metasedimentary formations and the calc-alkaline Lower Permian rhyolitic lavas.

Aplites and granitic porphyries with peralkaline affinity and rhyolitic composition, together with a little E-W oriented alkali dolerite, intrude the granodiorite and monzogranite of the calcalkaline association *s.s.* south of Mt. Cinto (Calasima, see fig. 1).

Only occasionally were dykes cutting the metamorphic basement observed.

Basic dykes with fine grain size are dark grey when fresh. Alteration is greater than in the acidic ones. Contacts with the host rock are clearcut and linear, and the grain size becomes coarser from the walls to the core of the dyke. They range in thickness from a dozen centimetres to ten meters at most and are generally subvertical.

Among the acidic dykes, generally light grey in colour, aplite, microgranite and granitic porphyry may be identified on the basis of mineral sizes and phenocrysts. They are frequently more than 200-300 m long. Acidic masses with cupola-like structures sometimes

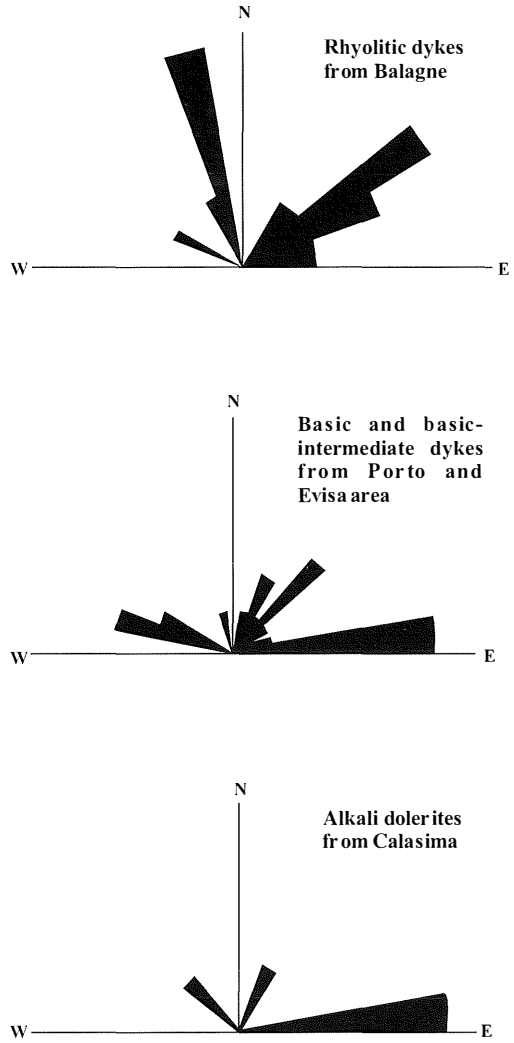

Fig. 2 - Outcropping strike directions of dykes from NW Corsica.

outcrop: they have non-linear walls and may reach widths of 20 to 30 m along the crosscut.

Since no dykes display large-scale deformational structures or schistosity associated with minerals, the NW Corsica dykes were probably not affected by the Hercynian metamorphic events but only by post-emplacement propylitic hydrothermal activity (Ottaviani *et al.*, 1989).

CLASSIFICATION, PETROGRAPHY AND MINERAL CHEMISTRY

Petrographic investigation highlighted the difficulty of classifying these dykes on a modal basis, both due to the very fine grain size of most lithotypes, mainly the basic ones, and to the different textures observed within the same petrographic groups.

The classification problem has been solved (Traversa *et al.,* 1997, and references therein) using chemical classifications (C.I.P.W. norm; T.A.S., Le Maitre *et al.,* 1989; R1-R2, De La Roche *et al.,* 1980) combined with petrography and mineral chemistry.

The C.I.P.W. norm of basic rocks, considering the occurrence of autometasomatic alterations, was calculated assuming a normalizing value of 0.15 for the Fe_2O_3/FeO ratio.

The basic-intermediate dykes shown in fig. 3 define two distinct trends, alkaline and calc-alkaline. The former contains lithotypes ranging in composition from basalt to trachybasalt (TchB) up to basaltic-trachyandesite (TchBA); the latter basaltic-andesite (BA) and andesite (A). Fig. 4 also identifies basaltic dykes with transitional affinity, plotting in the olivine-basalt and lati-basalt fields, hereafter simply referred to as transitional basalts (TrB). The basaltic dykes, when characterized by sub-ophitic textures and larger grain size, may be considered as microgabbros. Their position in the hawaiitic field of fig. 4 testifies a light evolved character; however, these have been assigned to the alkali basalt (AB) group taking also into account the occurence of kaersutite-pargasite amphibole and the presence of nefeline in the C.I.P.W. norm (see Tab. 10).

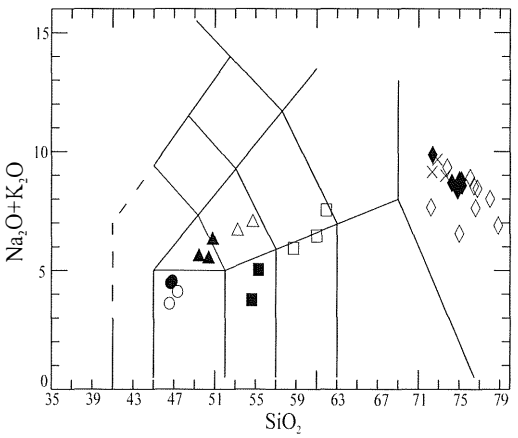

Fig. 3 - Distribution of NW Corsica dyke rocks in total Alkali *vs.* Silica (TAS) diagram (after Le Maitre, 1989). Symbols: solid circles: alkali basalt (AB); empty circles: transitional basalt (TrB); solid squares: basaltic andesite (BA); empty squares: andesite (A); solid triangles: trachybasalt (TchB); empty triangles: basaltic-trachyandesite (TchBA); solid diamonds: peralkaline rhyolite (PAR); empty diamonds: biotitic rhyolite (R); *x:* peraluminous rhyolite (PR).

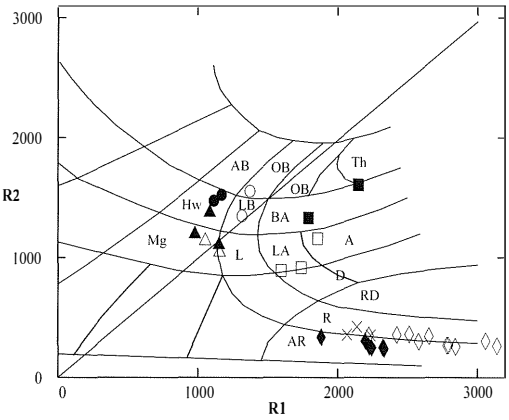

Fig. 4 - Distribution of NW Corsica dyke rocks in R1-R2 diagram (after De La Roche *et al.*, 1980), R1: 4Si -11 (Na+K) - 2 (Fe+Ti); R2: 6Ca + 2Mg +Al. Abbreviations: AB: alkali basalt; OB: olivine basalt; Th: tholeiite; Hw: hawaiite; LB: lati-basalt; BA: basaltic andesite; Mg: mugearite; L: latite; LA: lati-andesite; A: andesite; D: dacite; RD: rhyodacite; R: rhyolite; AR: alkali rhyolite. Symbols as in fig. 3.

Acidic dykes are represented by rocks of rhyolitic composition (figs. 3, 4), distinguished on a petrographic basis into aplite, microgranite, granitic porphyry and rocks characterized by rapid cooling textures. Mineral chemistry identified three different groups: granitic porphyries and aplite with sodic amphibole and aegirine (peralkaline rhyolite-PAR); microgranites with primary muscovite and biotite (peraluminous rhyolite-PR); and granitic porphyries and microgranite with biotite laths and secondary muscovite (biotitic rhyolite-R).

It should be noted that there is a compositional gap between andesitic and rhyolitic compositions, the dacitic-rhyodacitic type being virtually absent (figs. 3, 4).

TABLE 1

Microprobe compositions of representative feldspars from NW Corsica basaltic and calc-alkaline dyke rocks.

	1	2	3	4	5	6	7	8	9	10	11	12	13	14	15	16	17	18	19
	AB	AB	TrB	TrB	TchB	TchB	TchB	TchB	TchB	TchBA	BA	BA	BA	BA	BA	BA	A	A	A
	CB12	CB12	CB89	CB89	CB21	CB21	CB21	CB21	CB66	CB108	CB102	CB102	CB130	CB130	CB130	CB130	CB120	CB120	CB120
	A	B	B a	B b	A a	A b	B a	B b	A	A Ph	A	gm	Ac	A r	B a	B b	A c	A r	gm
SiO_2	67.66	56.67	65.30	65.05	65.01	67.42	64.92	66.86	68.36	64.83	52.98	59.80	55.00	63.09	62.65	54.69	57.36	63.24	62.88
Al_2O_3	20.50	25.97	21.65	18.95	17.99	20.39	18.47	20.95	19.83	22.52	29.59	25.67	28.69	23.12	23.82	28.69	24.35	23.29	23.31
FeO	0.15	1.46	0.19	0.04	0.11	0.16	0.06	0.10	0.14	0.08	0.14	0.10	0.24	0.09	0.21	0.21	1.72	0.34	0.40
MgO	0.02	0.01	0.42	n.d.	n.d.	0.02	n.d.	n.d.	0.01	0.01	0.01	0.03	0.04	n.d.	0.12	0.07	0.69	n.d.	n.d.
CaO	0.75	9.88	1.94	0.02	0.03	1.28	0.09	1.52	0.36	2.23	12.17	6.51	10.66	3.91	3.18	10.73	7.67	4.59	4.57
Na_2O	11.66	5.94	10.38	0.30	0.25	10.98	0.58	10.78	11.46	10.04	4.50	7.59	5.62	9.51	8.66	5.11	6.92	8.41	8.63
K_2O	0.09	0.29	0.26	16.34	16.61	0.16	15.85	0.18	0.09	0.43	0.04	0.48	0.26	0.12	1.30	0.29	0.72	0.54	0.32
Total	100.83	100.22	100.14	100.70	100.00	100.41	99.97	100.39	100.25	100.14	99.43	100.18	100.51	99.84	100.00	99.79	99.43	100.41	100.11
Si	11.770	10.240	11.481	11.937	12.038	11.775	11.985	11.689	11.923	11.399	9.641	10.64	9.881	11.177	11.110	9.884	10.417	11.155	11.130
Al	4.200	5.526	4.483	4.095	3.923	4.194	4.016	4.313	4.073	4.663	6.341	5.38	6.070	4.824	4.974	6.106	5.208	4.838	4.859
Fe^{3+}	0.022	0.221	0.028	0.006	0.017	0.023	0.009	0.015	0.020	0.012	0.021	0.015	0.036	0.013	0.031	0.032	0.261	0.050	0.059
Mg	0.005	0.006	0.110			0.005			0.003	0.003	0.003	0.008	0.011		0.032	0.019	0.187		
Ca	0.140	1.913	0.365	0.004	0.006	0.240	0.018	0.285	0.067	0.420	2.373	1.24	2.052	0.742	0.604	2.078	1.492	0.867	0.867
Na	3.933	2.081	3.539	0.107	0.090	3.718	0.208	3.654	3.876	3.423	1.558	2.62	1.958	3.267	2.978	1.791	2.437	2.877	2.962
K	0.020	0.067	0.058	3.825	3.924	0.036	3.733	0.040	0.020	0.096	0.009	0.109	0.060	0.027	0.294	0.067	0.167	0.122	0.072
Cations	20.090	20.054	20.064	19.974	19.998	19.991	19.969	19.996	19.982	20.016	19.976	20.012	20.070	20.050	20.023	19.977	20.169	19.909	19.949
Ab wt%	96.1	51.2	89.3	2.7	2.2	93.1	5.3	91.8	97.8	86.9	40.0	66.0	48.1	80.9	76.8	45.5	59.5	74.4	75.9
An wt%	3.4	47.1	9.2	0.1	0.1	6.0	0.5	7.2	1.7	10.7	59.8	31.3	50.4	18.4	15.6	52.8	36.4	22.4	22.2
Or wt%	0.5	1.6	1.5	97.2	97.6	0.9	94.3	1.0	0.5	2.4	0.2	2.7	1.5	0.7	7.6	1.7	4.1	3.2	1.8

Atomic proportions based on 32 oxygens. AB: alkali basalt; TrB: transitional basalt; TchB: trachybasalt; TchBA: basaltic trachy-andesite; BA: basaltic-andesite; A: andesite. A and B: different crystals; c: core; r: rim; gm: groundmass; Ph: phenocrysts; a and b: parts of the same crystal.

Alkaline (AB) and transitional (TrB) basaltic dykes

These are very similar lithotypes, texturally represented by intergranular and sometimes sub-ophitic rocks. The main differences are the occurrence of kaersutitic-pargasitic amphibole and normative Ne only in AB; moreover, pseudomorphs made up of chlorite and epidote aggregates, often rimmed by coronas of opaque minerals, and chloritized biotite laths, are also only found in AB. Clinopyroxene of the same composition is the dominant mafic mineral in both lithotypes; plagioclase and ilmenite complete the primary paragenesis.

The weak porphyritic texture of TrB is due to rare phenocrysts of plagioclase. The grain size, generally doleritic in samples from the core of the dykes, becomes finer toward the walls.

Plagioclase in both AB and TrB is represented by a quasi-pure albite (Ab_{89-96}, an. 1 and 3 of Table 1 and fig. 5A), most probably of subsolidus origin from a primary and more calcic plagioclase (Ab_{51}-An_{47}, an. 2 of Table 1 and fig. 5A) of which few relicts remain. Plagioclase is frequently affected by extensive saussurization and also speckled by white mica. In addition, TrB albite crystals are inhomogeneous in composition due to the presence of small areas of K-feldspar (Or_{97}-Ab_3, an. 4 of Table 1 and fig. 5A), undetectable under the microscope, probably representing a product of subsolidus unmixing. Interstitial K-feldspar crystallizes as final liquidus only in TrB; its composition is characterized by the complete lack of anorthite (Or_{91}-Ab_9, an. 1 of Table 2 and fig. 5A).

Clinopyroxene, more or less pinkish depending on its TiO_2 content, ranges in composition from diopside to a slightly

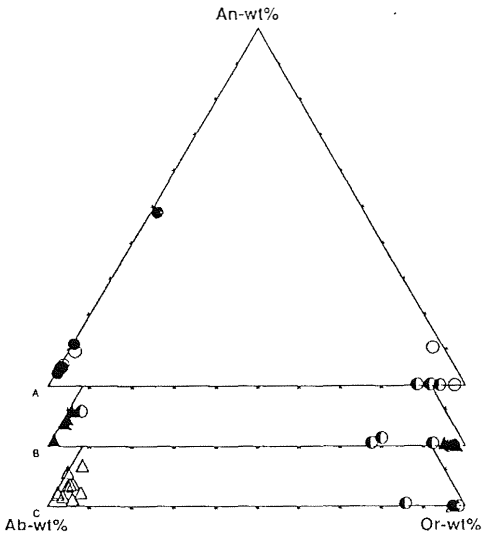

Fig. 5 - Feldspar microprobe compositions from NW Corsica basaltic dyke rocks in An-Ab-Or system. A: feldspars from alkali and transitional basalts; B: feldspars from trachybasalts; C: feldspars from basaltic-trachyandesites. Half-full circle: groundmass feldspar. Symbols as in fig. 3.

TABLE 2

Microprobe compositions of representative groundmass K-feldspar from NW Corsica dyke rocks.

	1	2	3	4	5	6
	TrB	**TchB**	**TchBA**	**A**	**PAR**	**PAR**
	CB89	**CB66**	**CB108**	**CB120**	**CB100**	**CB25**
SiO_2	64.32	64.76	65.42	64.60	64.82	65.38
Al_2O_3	18.90	18.71	18.50	18.48	18.65	18.49
FeO	0.59	1.24	0.12	0.16	0.45	0.14
MgO	0.10	0.40	n.d.	n.d.	0.03	n.d.
CaO	0.08	0.15	n.d.	0.07	n.d.	0.02
Na_2O	0.97	2.56	0.30	1.29	0.24	0.19
K_2O	15.25	12.72	15.98	15.12	16.14	16.56
Total	100.21	100.54	100.32	99.72	100.33	100.78
Si	11.864	11.833	12.020	11.945	11.951	11.998
Al	4.106	4.026	4.003	4.024	4.049	3.996
Fe^{3+}	0.091	0.189	0.018	0.025	0.069	0.021
Mg	0.027	0.109			0.008	
Ca	0.016	0.029		0.014		0.004
Na	0.347	0.907	0.107	0.462	0.086	0.068
K	3.589	2.965	3.746	3.567	3.796	3.877
Cations	20.040	20.058	19.894	20.037	19.959	19.964
Ab wt%	8.8	23.3	2.8	11.4	2.2	1.7
An wt%	0.4	0.7		0.3		0.1
Or wt%	90.8	76.0	97.2	88.2	97.8	98.2

Atomic proportions based on 32 oxygens. TrB: transitional basalt; TchB: trachybasalt; TchBA: basaltic trachy-andesite; A: andesite; PAR: peralkaline rhyolite.

TABLE 3

Microprobe compositions of representative clinopyroxenes from NW Corsica dyke rocks.

	1	2	3	4	5	6	7	8	9	10	11	12	13	14	15	16	17	18	19	20
	AB	**AB**	**AB**	**AB**	**TrB**	**TrB**	**TchB**	**TchB**	**TchB**	**TchBA**	**TchBA**	**TchBA**	**TchBA**	**BA**	**BA**	**PAR**	**PAR**	**PAR**	**PAR**	**PAR**
	CB12	**CB12**	**CB16**	**CB16**	**CB89**	**CB89**	**CB21**	**CB21**	**CB66**	**CB18**	**CB18**	**CB108**	**CB108**	**CB130**	**CB130**	**CB100**	**CB100**	**CB27**	**CB27**	**CB25**
	A c	A r	A c	A r	Ac	Ar	A c	A r	gm	A Ph c	A Ph r	A Ph c	A Ph r	A	B	A Ph c	A Ph r	A Ph c	A Ph r	gm
SiO_2	48.38	50.09	46.61	48.49	44.87	46.63	48.16	48.86	46.54	51.32	49.29	51.96	52.25	51.24	52.17	50.95	50.87	53.02	52.53	53.02
TiO_2	2.29	1.48	3.34	2.10	3.76	3.40	2.38	1.89	3.25	0.85	1.57	0.90	0.72	0.84	0.75	0.11	0.54	0.58	0.63	0.91
Al_2O_3	5.10	3.61	5.77	4.07	6.1	5.70	5.37	4.11	5.45	2.04	4.37	2.12	1.32	2.11	1.55	0.56	1.07	0.57	0.44	0.51
Cr_2O_3	0.08	0.07	n.d.	n.d.	0.05	0.05	0.30	0.05	0.02	0.07	0.04	0.16	n.d.	0.04	0.02	n.d.	n.d.	n.d.	n.d.	0.04
FeO	10.30	10.91	10.97	11.10	12.76	12.43	9.28	11.06	11.58	10.31	11.41	9.72	11.08	10.28	10.09	21.75	17.61	30.3	30.15	29.46
MnO	0.27	0.29	0.21	0.28	0.34	0.21	0.25	0.24	0.30	0.29	0.31	0.23	0.26	0.31	0.26	0.83	0.80	0.03	0.14	0.11
MgO	13.12	12.95	12.02	12.36	10.01	10.25	13.45	13.31	11.83	16.17	13.92	16.13	15.9	14.62	15.89	7.84	9.26	0.06	0.10	n.d.
CaO	20.59	21.09	21.36	20.71	20.73	20.63	19.92	19.78	20.15	17.97	18.46	18.13	17.39	20.27	18.88	18.07	19.54	0.08	0.47	0.58
Na_2O	0.55	0.46	0.64	0.46	0.66	0.64	0.42	0.42	0.58	0.34	0.52	0.30	0.30	0.12	0.17	0.27	0.42	14.15	13.75	13.53
Total	100.68	100.95	100.92	99.57	99.28	99.94	99.53	99.72	99.70	99.36	99.89	99.65	99.22	99.83	99.78	100.38	100.11	98.79	98.21	98.21
Si^{IV}	1.797	1.861	1.737	1.831	1.721	1.774	1.806	1.836	1.761	1.913	1.843	1.931	1.957	1.916	1.942	1.995	1.966	1.981	1.980	2.002
Al^{IV}	0.203	0.139	0.253	0.169	0.276	0.226	0.194	0.164	0.239	0.087	0.157	0.069	0.043	0.084	0.058	0.005	0.034	0.019	0.020	
Al^{VI}	0.020	0.019		0.012	0.000	0.029	0.043	0.018	0.004	0.003	0.035	0.024	0.016	0.009	0.009	0.021	0.015	0.006		0.023
Ti	0.064	0.041	0.094	0.060	0.108	0.097	0.067	0.053	0.093	0.024	0.044	0.025	0.02	0.024	0.021	0.003	0.016	0.016	0.018	0.026
Cr	0.002	0.002			0.002	0.002	0.009	0.001	0.001	0.002	0.001	0.005		0.001	0.001					0.001
Fe^{3+}	0.092	0.068	0.122	0.071	0.109	0.047	0.038	0.068	0.091	0.059	0.07	0.012	0.009	0.036	0.018		0.019	0.945	0.948	0.911
Fe^{2+}	0.228	0.270	0.209	0.279	0.297	0.349	0.252	0.280	0.275	0.263	0.287	0.29	0.338	0.286	0.296	0.712	0.550			
Mg	0.726	0.717	0.668	0.696	0.572	0.581	0.752	0.746	0.667	0.899	0.776	0.894	0.888	0.815	0.882	0.458	0.534	0.003	0.006	
Mn	0.008	0.009	0.007	0.009	0.011	0.007	0.008	0.008	0.010	0.009	0.01	0.007	0.008	0.010	0.008	0.028	0.026	0.001	0.004	0.004
Ca	0.819	0.839	0.853	0.838	0.852	0.841	0.800	0.796	0.817	0.718	0.739	0.722	0.698	0.812	0.753	0.758	0.809	0.003	0.019	0.023
Na	0.040	0.033	0.046	0.034	0.049	0.047	0.031	0.031	0.043	0.025	0.038	0.022	0.022	0.009	0.012	0.020	0.031	1.025	1.005	0.990
Cations	4.00	4.00	3.99	4.00	4.00	4.00	4.00	4.00	4.00	4.00	4.00	4.00	4.00	4.00	4.00	4.00	4.00	4.00	4.00	3.98
Wo	43.72	44.07	45.63	44.26	46.18	46.09	43.23	41.98	43.91	36.86	39.29	37.50	35.95	41.47	38.47	38.77	41.75			
En	38.76	37.65	35.73	36.75	31.03	31.86	40.62	39.30	35.87	46.16	41.23	46.43	45.74	41.61	45.06	23.4	27.53			
Fs	17.52	18.27	18.65	18.99	22.78	22.05	16.15	18.72	20.21	16.98	19.47	16.07	18.31	16.92	16.47	37.83	30.72			
Mg*	68.88	67.39	66.40	65.97	57.84	59.04	71.62	67.70	63.95	73.09	67.89	74.31	71.44	71.05	73.26	38.23	47.30			

Atomic proportions based on 6 oxygens. Fe^{+2}/Fe^{+3} partitioning according to Papike *et al.* (1974) for calcic clinopyroxenes; in PAR sodic clinopyroxene, total iron is Fe^{+3}.
AB: alkali basalt; TrB: transitional basalt; TchB: trachybasalt; TchBA: basaltic trachy-andesite; BA: basaltic-andesite; R: biotitic rhyolite; PAR: peralkaline rhyolite. A and B: different crystals; Ph: phenocrysts; c: core; r: rim; gm: groundmass.

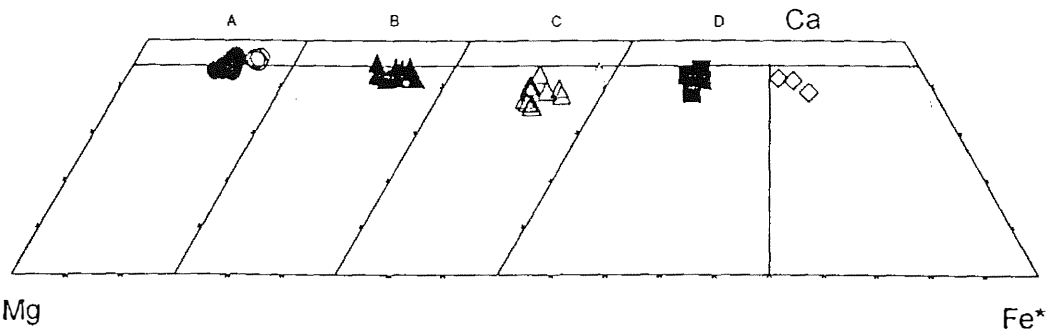

Fig. 6 - Clinopyroxene microprobe compositions from NW Corsica dyke rocks in Ca-Mg-Fe* ($Fe^*=Fe^{2+}+Fe^{3+}+Mn$) classification diagram (after Morimoto, 1988). Symbols as in fig. 3. Empty diamonds: PAR.

titaniferous augite (Wo_{46-44}-En_{31-39}-Fs_{23-17}, an. 5 and 1 of Table 3 and fig. 6A). Evolution from core to rim is marked by Al_2O_3 and TiO_2 decrease (an. 1-2, 3-4 and 5-6 of Table 3) whereas CaO content shows a slight increase (fig. 6A), typical of alkaline trends. Fig. 7 confirms the prevailing alkaline affinity of TrB and AB clinopyroxene.

Crystallization of kaersutite-pargasite amphibole and ilmenite accounts for the lower TiO_2 and FeO contents in AB compared with TrB clinopyroxene (an. 1-6, Table 3), whole-rock TiO_2 and FeOtot being comparable (see Table 10). Kaersutite (an. 1-2, Table 4 and fig. 8) is typically associated with primary ilmenite, which is also frequently observed as exsolution lamellae within subhedral titanite crystals. Fibrous pale green amphibole replacing augite crystals is observed in both AB and TrB; this is compositionally represented by actinolite-ferroactinolite (fig. 8).

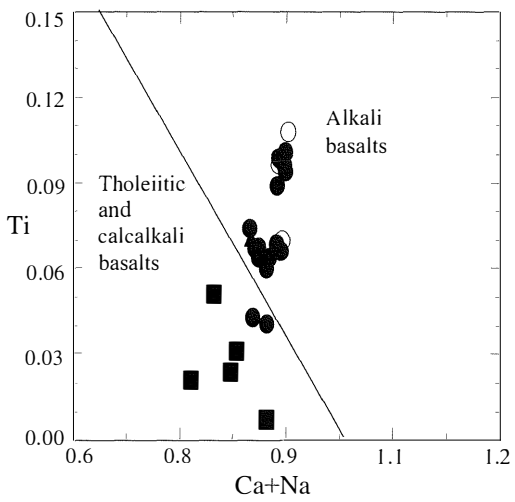

Fig. 7 - Discrimination diagram for basalts after *cpx* phenocryst compositions (after Leterrier *et al.*, 1982). Symbols as in fig. 3.

Ilmenite composition varies mainly due to its MnO content, higher in AB (average 2.52%) and lower in TrB (0.67%), whereas FeO and TiO_2 contents are broadly comparable (an. 1-4 of Table 5). Most common accessory phases in both AB and TrB are apatite and titanite, the latter most probably occurring as a late magmatic phase. Moreover, subordinate baddeleyite (ZrO_2) and very small zircon crystals (around 20 micrometres) were detected by electron microprobe at the Department of Geology, University of California, Berkeley. Searching for Zr mineral phases in AB and TrB was directed toward dating these rocks by the U-Pb method.

Trachybasaltic (TchB) and basaltic-trachyandesite (TchBA) dykes

In these rocks, relatively elongated subhedral plagioclase forms a framework, and the more equidimensional, smaller and subhedral augitic clinopyroxene fits in between. Augite crystals may also be elongated and, in this case, develop into a fan-shaped arrangement together with plagioclase. The grain size of minerals varies greatly, from almost sub-aphyric rocks,

TABLE 4

Microprobe compositions of representative calcic amphiboles from NW Corsica basaltic and calcalkaline dyke rocks.

	1	2	3	4	5	6	7	8	9	10	11	12	13	14
	AB	**AB**	**BA**	**BA**	**BA**	**BA**	**BA**	**BA**	**BA**	**BA**	**BA**	**A**	**A**	**A**
	CB12	**CB12**	**CB130**	**CB130**	**CB130**	**CB130**	**CB130**	**CB130**	**CB102**	**CB102**	**CB102**	**CB120**	**CB120**	**CB120**
	A	B	A	B c	B r	C c	C m	C r	A	B	Co	A Ph c	A Ph r	gm
SiO_2	41.10	40.50	45.00	43.39	44.08	43.81	49.99	53.68	50.50	49.95	51.77	46.71	47.82	47.13
TiO_2	4.67	4.54	1.62	2.25	2.09	2.62	0.83	0.05	0.09	0.17	0.43	1.29	1.06	1.33
Al_2O_3	12.54	11.96	8.01	9.95	9.30	9.64	3.03	2.27	6.04	6.57	4.60	6.48	5.90	6.32
Cr_2O_3	0.07	n.d.	0.04	n.d.	0.03	n.d.	n.d.	n.d.	0.67	0.33	0.11	0.15	0.16	0.13
FeO	16.12	16.36	19.71	18.04	19.08	17.46	23.64	16.66	10.94	12.36	11.41	16.96	16.36	16.85
MnO	0.31	0.27	0.38	0.29	0.31	0.11	0.39	0.36	0.33	0.36	0.44	0.21	0.26	0.36
MgO	10.43	10.45	10.95	11.45	10.90	11.85	10.46	13.40	15.89	15.04	16.35	12.15	12.55	12.25
CaO	11.24	11.04	9.80	10.45	10.47	10.55	9.32	12.45	12.41	12.37	12.09	11.36	11.76	11.63
Na_2O	2.83	2.89	2.19	2.36	2.54	2.40	0.31	0.11	0.59	0.78	0.59	1.43	1.31	1.36
K_2O	0.69	0.82	0.57	0.69	0.62	0.57	0.26	0.08	0.13	0.26	0.12	0.78	0.69	0.73
Total	100.00	98.83	98.27	98.87	99.42	99.01	98.23	99.06	97.59	98.19	97.91	97.52	97.87	98.09
Si	6.040	6.040	6.694	6.400	6.500	6.433	7.488	7.738	7.214	7.150	7.367	6.952	7.073	6.974
Al^{IV}	1.960	1.960	1.306	1.600	1.500	1.567	0.512	0.262	0.786	0.850	0.633	1.048	0.927	1.026
sumT	8.000	8.000	8.000	8.000	8.000	8.000	8.000	8.000	8.000	8.000	8.000	8.000	8.000	8.000
Al^{VI}	0.212	0.143	0.098	0.129	0.117	0.101	0.022	0.124	0.231	0.259	0.138	0.089	0.101	0.077
Ti	0.516	0.509	0.181	0.250	0.232	0.289	0.094	0.005	0.010	0.018	0.046	0.144	0.118	0.148
Fe^{3+}	0.147	0.177	0.552	0.547	0.485	0.493	0.247	0.112	0.381	0.362	0.368	0.297	0.215	0.276
Cr	0.008	0.000	0.005	0.000	0.003	0.000	0.000	0.000	0.076	0.037	0.012	0.018	0.019	0.015
Mg	2.285	2.324	2.429	2.518	2.396	2.594	2.336	2.880	3.384	3.210	3.469	2.696	2.768	2.703
Fe^{2+}	1.830	1.847	1.736	1.556	1.767	1.522	2.301	1.878	0.919	1.113	0.966	1.755	1.779	1.781
Mn	0.000	0.000	0.000	0.000	0.000	0.000	0.000	0.000	0.000	0.000	0.000	0.000	0.000	0.000
sumC	5.000	5.000	5.000	5.000	5.000	5.000	5.000	5.000	5.000	5.000	5.000	5.000	5.000	5.000
Mg	0.000	0.000	0.000	0.000	0.000	0.000	0.000	0.000	0.000	0.000	0.000	0.000	0.000	0.000
Fe^{2+}	0.003	0.016	0.165	0.122	0.101	0.129	0.413	0.018	0.007	0.004	0.023	0.059	0.029	0.028
Mn	0.039	0.034	0.048	0.036	0.039	0.014	0.049	0.044	0.040	0.044	0.053	0.026	0.033	0.045
Ca	1.770	1.764	1.562	1.651	1.654	1.660	1.496	1.923	1.899	1.897	1.843	1.812	1.864	1.844
Na	0.188	0.185	0.225	0.190	0.206	0.198	0.042	0.015	0.054	0.055	0.081	0.103	0.075	0.083
sumB	2.000	2.000	2.000	2.000	2.000	2.000	2.000	2.000	2.000	2.000	2.000	2.000	2.000	2.000
Na	0.618	0.650	0.406	0.485	0.520	0.485	0.048	0.015	0.110	0.162	0.082	0.309	0.301	0.307
K	0.129	0.156	0.108	0.130	0.117	0.107	0.050	0.015	0.024	0.047	0.022	0.148	0.130	0.138
sumA	0.748	0.806	0.514	0.615	0.637	0.592	0.098	0.030	0.133	0.209	0.104	0.458	0.431	0.445
oxygens	22.93	22.91	22.72	22.73	22.76	22.75	22.88	22.94	22.81	22.82	22.82	22.85	22.89	22.86
Mg*	53.09	52.83	49.28	52.68	50.05	54.59	43.69	58.39	71.53	67.82	71.09	55.78	57.37	55.92

Atomic proportions are based on an anhydrous basis per 23 oxygens and on different cation sum to account for minimum and maximum ferric estimate according to Schumacher (1997); Fe^{+2}/Fe^{+3} partitioning is given as an average of the minimum and the maximum ferric estimates (Schumacher, 1997). Classification is according to Leake (1997).
AB: alkali basalt; BA: basaltic-andesite; A: andesite. A and B: different crystals; Ph: phenocrysts; c: core; r: rim; m: mantle; gm: groundmass; Co: coronitic amphibole; 1-2: kaersutite; 3-7: magnesiohastingsite; 8: actinolite; 9-14: magnesiohornblende.

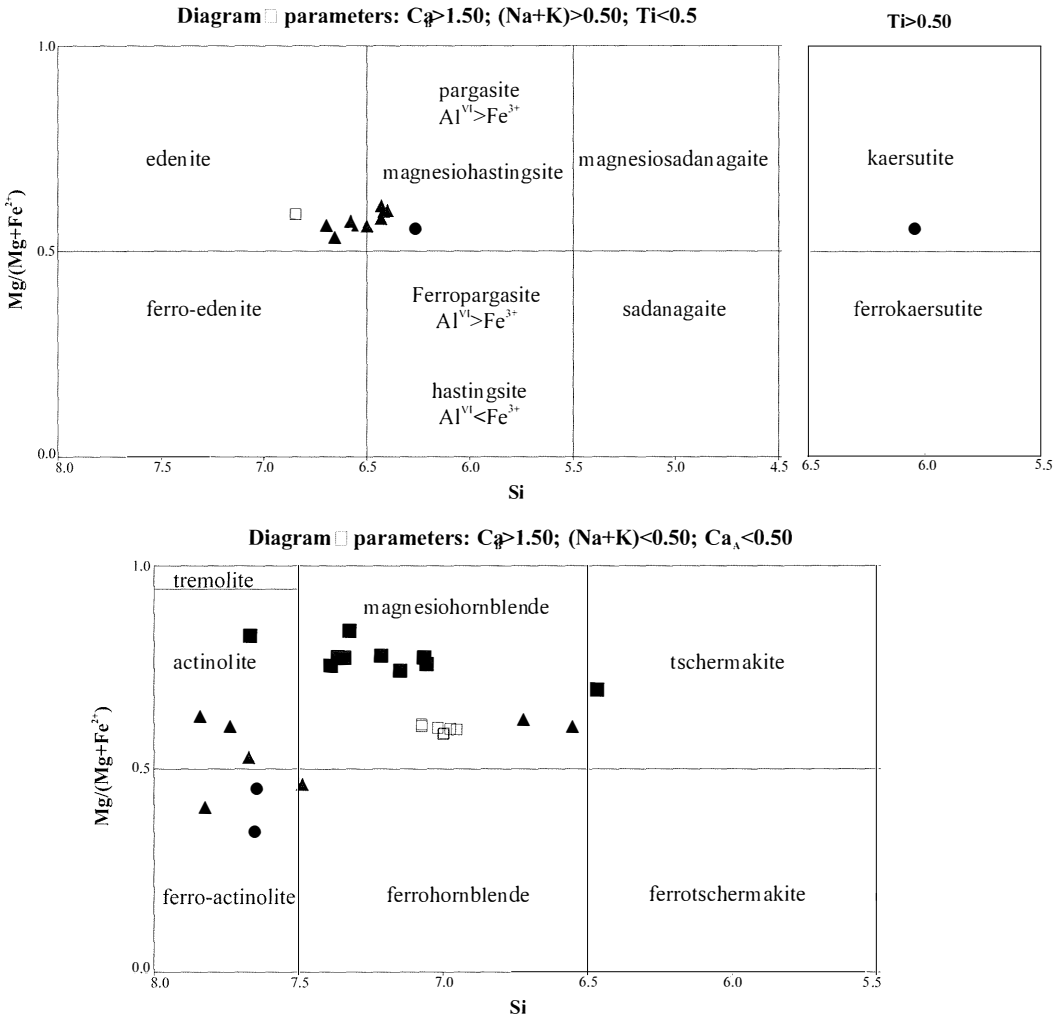

Fig. 8 - Calcic amphibole microprobe compositions from NW Corsica dyke rocks in $Mg/Mg+Fe^{+2}$ *vs.* Si classificative diagram (after Leake *et al.*, 1997). Symbols: solid circles: alkali basalt; full squares: basaltic andesite without *cpx*; full triangles: basaltic andesite with *cpx*; empty squares: andesite.

fluidal due to the iso-orientation of plagioclase laths, to rocks of medium grain size. Clinopyroxene is also present in the groundmass as microcrysts which grew during the final rapid stage of magma cooling, together with green calcic amphibole. K-feldspar and quartz are found interstitially. Opaque minerals complete the paragenesis. Fresh calcic amphibole is to be found only in TchBA; in TchB it is completely transformed to chlorite. Xenocrysts of quartz, marginally resorbed and mantled by minute coronitic clinopyroxene, are present in TchB. Notably, plagioclase and clinopyroxene phenocrysts are present only in TchBA. The core of the latter is often replaced by microcrystalline chlorite.

TABLE 5

Microprobe compositions of representative ilmenites from NW Corsica dyke rocks.

	1 **AB** **CB12** A	2 **AB** **CB12** B	3 **AB** **CB12** C	4 **TrB** **CB89** gm	5 **TchB** **CB21** A	6 **TchBA** **CB18** A	7 **R** **CB96** A	8 **R** **CB96** B
SiO_2	0.84	n.d.	0.04	n.d.	0.01	0.96	0.09	n.d.
TiO_2	49.22	49.57	48.57	49.28	49.05	48.5	50.83	40.26
Al_2O_3	0.09	n.d.	0.31	n.d.	0.04	0.15	0.04	n.d.
FeO	45.17	48.6	46.97	50.29	46.05	45.53	43.94	58.17
Cr_2O_3	n.d.	n.d.	0.09	n.d.	0.04	n.d.	n.d.	n.d.
MnO	2.67	2.35	2.53	0.67	3.85	3.45	4.25	n.d.
MgO	0.05	0.04	0.07	n.d.	n.d.	n.d.	0.02	n.d.
CaO	1.39	0.01	0.02	0.35	0.17	1.05	n.d.	0.03
Total	99.43	100.6	98.6	100.6	99.21	99.64	99.17	98.46
Ti	0.952	0.945	0.944	0.940	0.947	0.940	0.978	0.804
Al	0.003		0.009		0.001	0.005	0.001	
Cr			0.002		0.001			
Fe^{+3}	0.045	0.055	0.045	0.060	0.051	0.055	0.021	0.196
Fe^{+2}	0.926	0.975	0.970	1.006	0.938	0.926	0.918	1.097
Mn	0.058	0.050	0.055	0.014	0.084	0.075	0.092	
Mg	0.002	0.002	0.003				0.001	
Ca	0.038		0.001	0.010	0.005	0.029		0.001
Cations	2.024	2.027	2.029	2.030	2.027	2.030	2.011	2.098

Atomic proportions based on 3 oxygens. SiO_2 treated as impurity; Fe^{+2}/Fe^{+3} partitioning according to Afifi and Essene (1988). AB: alkali basalt; TrB: transitional basalt; TchB: trachybasalt; TchBA: basaltic trachy-andesite; R: biotitic rhyolite. A, B, C: different crystals; gm: groundmass.

The plagioclase of both TchB and TchBA, a non-zoned albite (Ab_{87-98}, an. 6, 8-10 of Table 1), is characterized by speckles of K-feldspar (Or_{94-97}-Ab_{2-5}, an. 5 and 7 of Table1), sometimes also visible under the microscope, of the same kind detected in TrB plagioclase. The K-feldspar of the groundmass has a quite different composition, as the albite component can be significant: Or_{76-97}-Ab_{3-23} (an. 2-3 of Table 2). Feldspar compositions are plotted in fig. 5B-C.

Clinopyroxene is represented by augite (Wo_{36-44}-En_{46-36}-Fs_{18-20}, an. 13 and 19 of Table 3 and fig. 6B-C); its CaO and TiO_2 contents decrease from TchB to TchBA, matching the corresponding trend for whole-rock oxides (see Table 10). Mg* is fairly constant, but the MgO/FeO ratio decreases from core to rim (an. 10-11, 12-13 of Table 3) in line with proceeding crystallization. The increasing SiO_2 content from TchB to TchBA augite is linked to the more highly evolved character of the host rock.

TchB and TchBA are characterized by magnetite and ilmenite among the opaque minerals, accessory minerals being apatite, titanite and pyrite of large dimensions.

Basaltic-andesitic (BA) and andesitic (A) dykes

The dominant mineralogical phases, calcic amphibole and plagioclase, are set within microgranular-intergranular textures. Only in BA is augitic clinopyroxene occasionally present and the texture is sub-ophitic. The interstitial groundmass is made up of minute

crystals of subhedral plagioclase, amphibole, biotite, quartz and subordinate K-feldspar. Amphibole and biotite are often present as clusters, sometimes large.

Xenocrysts of quartz and more rarely of K-feldspar, bordered by minute crystals of calcic amphibole, are observed in both BA and A.

Tabular plagioclase defines the rare igneous lineation which is sometimes present in both BA and A, whereas porphyritic textures are occasionally present in A.

The clinopyroxene of BA is an augite (Wo_{38-41}-En_{45-42}-Fs_{16-17}, an. 15 and 14 of Table 3 and fig. 6D) characterized by lower contents of TiO_2 (average 0.95%) compared with AB and TrB, in line with the different affinity of the lithotypes (see fig. 7).

The amphibole of both A and clinopyroxene-lacking BA is represented by magnesiohornblende (Table 4 and fig. 8), whereas amphibole from BA with clinopyroxene ranges in composition from edenite to magnesiohastingsite (Table 4 and fig. 8). Magnesiohornblende from BA shows the highest Mg* number among all analysed calcic amphiboles, in line with the highest whole-rock Mg* among calc-alkaline dykes (see Table 10). Instead, the $Mg/(Mg+Fe^{+2})$ value of amphibole from BA with clinopyroxene is the lowest (fig. 8) because of the early crystallization of augite, which is also responsible for the lower CaO contents of BA magnesiohastingsite (see Table 4). Only a moderate zoning pattern is observed across amphibole crystals and between the phenocrysts and microcrysts of the groundmass. Secondary actinolitic amphibole (fig. 8), which either crystallizes at the rim of primary amphibole or replaces it completely, occurs frequently.

Biotite has Mg-rich compositions (an. 1-3 of Table 6). Fig. 9 shows the decreasing in the $Mg/(Mg+Fe^{VI})$ ratio and Al^{VI} from BA to A biotites; Fe^{+3} substitution for Al^{VI} is governed mainly by oxidation conditions.

Plagioclase phenocrysts show compositional zoning from labradorite (An_{50-53}, an. 13 and 16 of Table 1) to oligoclase (An_{16-18}, an. 15 and 14 of Table 1) in BA and from andesine (An_{37}, an. 17 of Table 1) to oligoclase (An_{22}, an. 18 of Table 1) in A. Groundmass plagioclase ranges from andesine (An_{31}, an. 12 of Table 1) in BA

TABLE 6

Microprobe compositions of representative biotites from NW Corsica calc-alkaline and rhyolitic dyke rocks.

	1	2	3	4	5
	BA	**BA**	**A**	**PR**	**PR**
	CB102	**CB102**	**CB120**	**CB70**	**CB70**
	A	B	gm	A Ph c	A Ph r
SiO_2	39.47	38.63	37.43	33.38	34.79
TiO_2	2.49	2.53	3.98	2.64	2.92
Al_2O_3	14.92	14.86	13.58	17.93	18.10
Cr_2O_3	0.54	0.70	0.13	n.d.	n.d.
FeO	15.23	14.57	19.12	25.24	23.44
MnO	0.16	n.d.	0.10	0.30	0.32
MgO	14.30	14.31	11.30	7.71	6.86
CaO	0.08	0.09	0.11	0.06	n.d.
Na_2O	0.24	0.21	0.06	0.08	0.09
K_2O	8.99	8.83	9.64	7.93	9.59
Total	96.42	94.73	95.45	95.27	96.11
Si	2.90	2.87	2.83	2.56	2.69
Al^{IV}	1.10	1.13	1.17	1.44	1.31
Z	4.00	4.00	4.00	4.00	4.00
Al^{VI}	0.19	0.18	0.05	0.18	0.34
Fe^{3+VI}	0.01	0.02	0.15	0.47	0.01
Ti	0.14	0.14	0.23	0.15	0.17
Cr	0.03	0.04	0.01		
Mg	1.56	1.59	1.28	0.88	0.79
Fe^{2+}	0.92	0.88	1.06	1.15	1.5
Mn	0.01		0.01	0.02	0.02
Y	2.86	2.85	2.79	2.85	2.83
Ca	0.01	0.01	0.01	0.01	
Na	0.03	0.03	0.01	0.01	0.01
K	0.84	0.84	0.93	0.78	0.95
W	0.88	0.88	0.95	0.80	0.96
Cations	7.74	7.73	7.74	7.65	7.79
Mgv	0.63	0.64	0.55	0.43	0.34

Recalculation according to Dymek (1983). BA: basaltic andesite; A: andesite; PR: peraluminous rhyolite. A and B: different crystals; Ph: phenocrysts; c:c ore; r: rim.

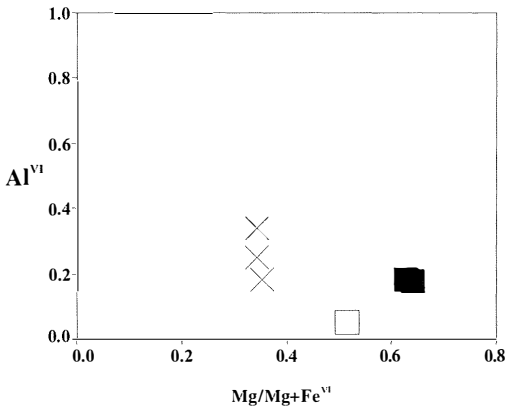

Fig. 9 - Biotite microprobe compositions from NW Corsica dyke rocks in Al^{VI} *vs.* $Mg/Mg+Fe^{VI}$ diagram. Symbols as in fig. 3.

to oligoclase (An_{22}, an. 19 of Table 1) in A. Interstitial K-feldspar, more widespread in A, is represented by Or_{88} (an. 4 Table 2). Feldspar compositions are plotted in fig. 10.

Magnetite is characterized by variable Cr_2O_3 contents (up to 9.1%) (an. 2-4 of Table 7). Instead, ilmenite, generally less widespread than magnetite and often included in calcic amphibole, is the only opaque present in BA with clinopyroxene.

Peraluminous rhyolitic dykes (PR)

These are exclusively represented by microgranites with autoallotriomorphic microgranular texture. The main mineralogical phases are quartz, sodic plagioclase,

TABLE 7

Microprobe compositions of representative magnetites from NW Corsica dyke rocks.

	1	2	3	4	5	6	7	8
	TchBA	**BA**	**BA**	**A**	**R**	**PAR**	**PAR**	**PAR**
	CB108	**CB102**	**CB102**	**CB120**	**CB96**	**CB100**	**CB100**	**CB105**
	A	gm	gm	A	A	gm	A	A
SiO_2	1.99	0.05	0.03	n.d.	n.d.	0.28	0.14	0.07
TiO_2	0.62	n.d.	n.d.	0.36	0.03	4.26	12.09	5.96
Al_2O_3	0.75	0.30	n.d.	0.29	0.08	0.10	1.13	0.02
Cr_2O_3	0.07	9.10	3.15	1.83	n.d.	n.d.	0.03	0.04
FeO	89.02	82.96	91.05	90.57	93.16	88.75	81.25	85.99
MnO	0.05	0.61	n.d.	n.d.	0.10	0.26	0.80	0.09
MgO	0.74	n.d.	n.d.	n.d.	n.d.	n.d.	0.11	n.d.
Total	93.24	93.02	94.23	93.05	93.37	93.65	95.55	92.17
Si	0.076	0.002	0.001			0.011	0.005	0.003
Ti	0.018			0.010	0.001	0.123	0.344	0.176
Al	0.034	0.014		0.013	0.004	0.005	0.050	0.001
Cr	0.002	0.279	0.095	0.056			0.001	0.001
Fe^{+3}	1.778	1.704	1.903	1.910	1.995	1.728	1.251	1.641
Fe^{+2}	1.050	0.982	1.001	1.010	0.998	1.125	1.317	1.175
Mn	0.002	0.020			0.003	0.008	0.026	0.003
Mg	0.042						0.006	
Cations	3.000	3.000	3.000	3.000	3.000	3.000	3.000	3.000
Ulvöspinel	1.92			1.04	0.09	12.45	34.55	17.61
Spinel	1.82	0.69		0.66	0.18	0.23	2.53	0.05
Chromite	0.11	13.95	4.75	2.79			0.04	0.06
Magnetite	96.15	85.36	95.25	95.51	99.73	87.32	62.87	82.28

Atomic proportions based on 4 oxygens; Fe^{+2}/Fe^{+3} partitioning according to Finger (1972). TchBA: basaltic trachy-andesite; BA: basaltic-andesite; A: andesite; R: biotitic rhyolite; PAR: peralkaline rhyolite. A: single crystal; gm: groundmass.

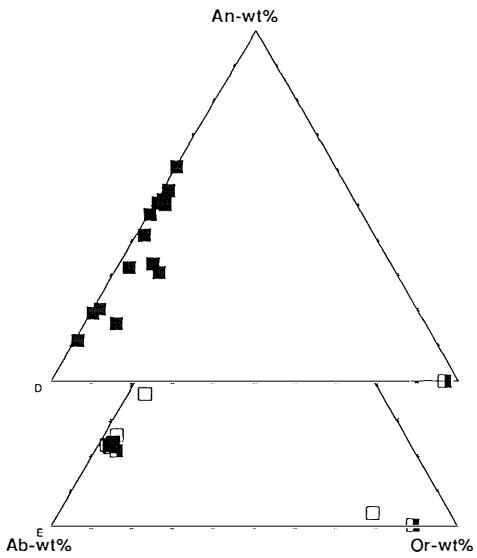

Fig. 10 - Microprobe compositions of feldspars from NW Corsica calc-alkaline dyke rocks in An-Ab-Or system. D: feldspars from basaltic andesite; E: feldspars from andesite. Half-full square: groundmass feldspar. Symbols as in fig. 3.

microcline, muscovite and Al^{VI}-rich biotite (an. 4 and 5 of Table 6 and fig. 9).

K-feldspar is an Or-rich (Or_{97}-Ab_3, an. 3 of Table 8), often perthitic (Or_{92}-Ab_8/Or_{10}-Ab_{88}, an. 4 and 5 of Table 8) anhedral poikilitic microcline.

Plagioclase, generally subhedral with sericitized cores, has albite and/or oligoclase compositions (Ab_{86-99}, an. 1-2, 6 of Table 8) with no significant zoning and with clear rims of late-stage crystallization. Synchronous discrete K and Na feldspars are typical of subsolvus granite. Feldspar compositions are plotted in fig. 11 A.

Opaque minerals are exclusively represented by magnetite; accessory phases are apatite, zircon and allanite.

Biotitic rhyolitic dykes (R)

These rocks are mainly represented by granitic porphyries and subordinate microgranites, together with rocks characterized by rapid cooling textures (e.g.: small masses of rhyolite from the Fango river, fig. 1). Quartz, sodic plagioclase, alkali feldspar and biotite are the main mineralogical phases. The groundmass shows either autoallotriomorphic or spherulitic textures, sometimes synchronous with granophyric intergrowths. Some R are characterized by discrete K and Na feldspars, plagioclase being present both as phenocrysts and in the groundmass or as an autoallotriomorphic phase in the microgranites (Ab_{91-96}, an. 7 and 8 of Table 8). Mesoperthitic alkali feldspar of intermediate composition is present in the remaining R samples. Mesoperthitic feldspar and quartz phenocrysts are resorbed to varying degrees and sometimes form large clusters, giving the rock a glomeroporphyritic texture. Biotite phenocrysts are dissected and replaced by interbedded muscovite, chlorite and epidote; microphenocrysts are often included in plagioclase and transformed into chlorite and iron oxides. Secondary white mica is also widespread interstitially and as flakes derived from the alteration of alkali feldspar. Opaque minerals of all R are represented by magnetite (an. 5 of Table 7); accessory phases are apatite

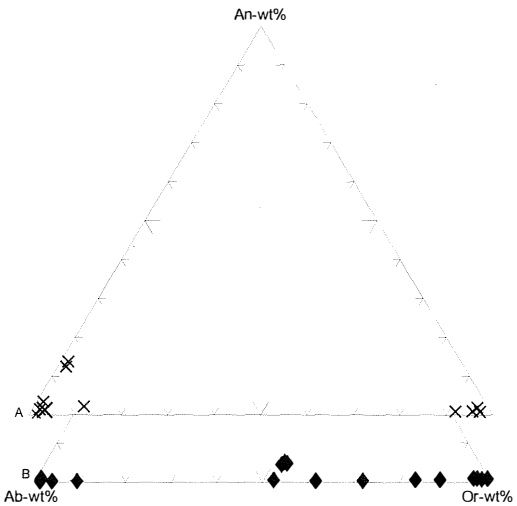

Fig. 11 - Microprobe compositions of feldspars from NW Corsica rhyolitic dyke rocks in An-Ab-Or system. A: feldspar from peraluminous rhyolite; B: feldspars from peralkaline rhyolite. Symbols as in fig. 3.

TABLE 8

Microprobe compositions of representative alkali feldspars from NW Corsica rhyolitic dyke rocks.

	1	2	3	4	5	6	7	8	9	10	11	12	13	14	15	16	17
	PR	**PR**	**PR**	**PR**	**PR**	**PR**	**R**	**R**	**PAR**	**PAR**	**PAR**	**PAR**	**PAR**	**PAR**	**PAR**	**PAR**	**PAR**
	CB68	**CB68**	**CB 68**	**CB70**	**CB70**	**CB70**	**CB96**	**CB96**	**CB100**	**CB100**	**CB100**	**CB100**	**CB100**	**CB100**	**CB100**	**CB26**	**CB26**
	A c	A r	B	A a	A b	B	A	B	A Ph a	A Ph b	B Ph a	B Ph b	C Ph a	C Ph b	gm	A Ph a	APh b
SiO_2	68.60	67.07	64.51	64.12	68.36	65.48	65.80	68.11	64.47	68.03	65.67	64.55	66.38	68.20	69.56	65.59	69.00
Al_2O_3	19.84	19.82	18.61	18.90	20.21	21.97	21.14	19.94	17.93	19.49	19.57	19.63	18.51	19.41	20.01	18.56	19.45
FeO	n.d.	0.07	n.d.	n.d.	0.01	0.02	0.32	0.02	0.42	0.02	0.14	0.16	0.20	n.d.	0.13	0.08	0.12
MgO	n.d.	n.d.	n.d.	0.03	n.d.	n.d.	0.10	n.d.	n.d.	0.03	n.d.	0.03	n.d.	n.d.	0.02	n.d.	n.d.
CaO	0.06	0.57	0.08	0.05	0.53	2.85	0.33	0.62	0.05	0.12	0.90	0.92	0.05	0.22	0.06	0.02	0.02
Na_2O	11.45	11.33	0.29	0.88	10.23	10.09	10.68	11.32	2.03	11.60	5.37	5.11	4.58	11.66	10.46	0.36	11.51
K_2O	0.08	0.14	17.06	15.09	1.69	0.19	1.31	0.10	14.68	0.17	9.07	9.12	10.41	0.20	0.60	16.22	0.06
Total	100.03	99.00	100.55	99.07	101.03	100.60	99.68	100.11	99.58	99.46	100.72	99.52	100.13	99.69	100.84	100.83	100.16
Si	11.949	11.853	11.920	11.913	11.886	11.464	11.637	11.897	11.962	11.954	11.799	11.743	12.004	11.962	12.017	12.002	12.014
Al	4.070	4.125	4.050	4.135	4.138	4.530	4.403	4.102	3.918	4.033	4.141	4.206	3.942	4.009	4.071	4.000	3.988
Fe^{+3}		0.010			0.001	0.003	0.047	0.003	0.065	0.003	0.021	0.024	0.030		0.019	0.012	0.017
Mg				0.008			0.026			0.008		0.008			0.005		
Ca	0.011	0.108	0.016	0.010	0.099	0.535	0.063	0.116	0.010	0.023	0.173	0.179	0.010	0.041	0.011	0.004	0.004
Na	3.867	3.882	0.104	0.317	3.449	3.425	3.662	3.834	0.730	3.952	1.871	1.803	1.606	3.965	3.504	0.128	3.886
K	0.018	0.032	4.022	3.577	0.375	0.042	0.296	0.022	3.475	0.038	2.079	2.117	2.402	0.045	0.132	3.786	0.013
Cations	19.915	20.010	20.112	19.960	19.948	19.999	20.134	19.974	20.160	20.011	20.084	20.080	19.994	20.022	19.759	19.932	19.922
Abwt%	99.3	96.5	2.5	8.1	87.9	85.6	91.1	96.5	17.3	98.5	45.4	44.0	40.0	97.9	96.1	3.3	99.6
Anwt%	0.3	2.7	0.4	0.3	2.5	13.4	1.6	2.9	0.2	0.6	4.2	4.4	0.2	1.0	0.3	0.1	0.1
Orwt%	0.5	0.8	97.1	91.6	9.6	1.0	7.4	0.6	82.4	0.9	50.4	51.6	59.8	1.1	3.6	96.6	0.3

Atomic proportions based on 32 oxygens. PR: peraluminous rhyolite; R: biotitic rhyolite; PAR: peralkaline rhyolite. A, B, C: different crystals; Ph: phenocrysts; a and b: parts of the same crystal; c: core; r: rim; gm: groundmass.

and zircon, the latter often metamictic. Rare fluorite was observed in only one sample.

Peralkaline rhyolitic dykes (PAR)

Texturally represented by porphyritic types and aplites, sometimes showing micrographic textures (micropegmatite), these rocks are characterized by sodic amphibole and aegirine, smaller in size than the associated mesoperthitic alkali feldspar and quartz. Mesoperthite compositions are represented by Or-rich (Or_{97}-Ab_3, an. 16 of Table 8) and albitic phases (Or_0-Ab_{100}, an. 17 of Table 8), whereas groundmass feldspar is almost exclusively potassic (Or_{98}-Ab_2, an. 6 of Table 2). Feldspar compositions are plotted in fig. 11 B. Reddening of feldspar due to minute inclusions of hematite is typical.

Sodic amphibole, strongly pleochroic from light yellow to deep blue, is present as both euhedral phenocrysts and anhedral microphenocrysts in the groundmass. Its composition, according to Leake's classification (Leake *et al.,* 1997), is represented by arfvedsonite and riebeckite (Table 9), although these are indistinguishable from their optical properties. The co-existence of these two amphiboles in such an acidic rock is generally ascribed to post-crystallization oxidation of Fe^{+2} to Fe^{+3}, probably through the action of oxidizing fluids in which riebeckite forms; however, the lack of petrographic evidence of late riebeckite crystallization indicates that its formation may simply be due to fO_2 variations in magmatic conditions.

Aegirine (an. 18-20 of Table 3), always anhedral and with resorbed rims, is very frequently associated with amphibole and sometimes crystallizes at its borders. This last feature indicates the later formation of pyroxene, possibly promoted by chemical disequilibrium between alkali amphibole and an oxidizing water-rich vapor phase, as suggested for the peralkaline granite of the Evisa and Bonifatto complexes (Bonin, 1988; Egeberg *et al.*, 1993).

The charge balance of the aegirine structural formula was calculated by considering total iron as Fe^{+3}; (Ca+Mg+Fe^{+2}) values are close to 0 whereas Na>1, typical of Na-pyroxenes (Morimoto, 1988).

The groundmass of porphyritic PAR is made up of autoallotriomorphic quartz and K-feldspar as well as amphibole, mostly

TABLE 9

Microprobe compositions of representative sodic amphiboles from NW Corsica peralkaline rhyolitic dyke rocks.

	1	2	3	4
	CB26	**CB27**	**CB27**	**CB105**
	gm	A	B	gm
SiO_2	51.36	51.42	50.28	50.37
TiO_2	1.10	0.86	1.05	1.84
Al_2O_3	0.37	0.60	0.63	0.49
FeO	34.99	34.60	34.44	31.68
MnO	0.54	0.38	0.42	0.85
MgO	0.49	0.00	0.05	0.00
CaO	0.08	0.61	0.89	0.39
Na_2O	6.62	7.86	8.33	7.87
K_2O	0.98	1.33	1.33	1.70
Total	96.53	97.66	97.42	95.19
Si	7.933	7.891	7.884	7.909
Al^{IV}	0.067	0.109	0.116	0.091
sumT	8.00	8.00	8.00	8.00
Al^{VI}	0.000	0.000	0.000	0.000
Ti	0.128	0.099	0.124	0.217
Fe^{3+}	1.948	1.931	1.357	1.796
Cr	0.000	0.000	0.000	0.004
Mg	0.113	0.000	0.012	0.000
Fe^{2+}	2.571	2.509	3.159	2.364
Mn	0.071	0.049	0.056	0.113
sumC	4.831	4.589	4.707	4.494
Ca	0.013	0.100	0.150	0.066
Na	1.982	1.900	1.850	1.934
sumB	2.00	2.00	2.00	2.00
Na	0.000	0.439	0.682	0.462
K	0.193	0.260	0.266	0.341
sumA	0.19	0.70	0.95	0.80

Atomic proportions based on Si+Al=8.00 (Hawthorne, 1982). A and B: different crystals; gm: groundmass. 1: riebeckite; 2-4: arfvedsonite.

riebeckite (see an. 1 of Table 9), and aegirine microcrysts. Acicular crystals of arfvedsonite (an. 4 of Table 9) and K-feldspar sometimes form good examples of spherulite growing around quartz phenocrysts.

Some samples of granitic porphyries characterized by ferroaugitic clinopyroxene are also included in this group, despite their probably non-primary metalluminous character (A.I.=0.94), on the basis of the affinities of trace elements and REE patterns (see fig. 15 and 20). Mesoperthitic alkali feldspar, as in peralkaline PAR, displays a wide compositional range, from Or-rich (Or_{82}-Ab_{17}, an. 9 of Table 8) and intermediate (Or_{50-60}-Ab_{45-40}, an. 11-13 of Table 8) up to Ab-rich (Or_1-Ab_{98}, an. 10 and 14 of Table 8), typical of hypersolvus granite. Microperthitic alkali feldspar (Or_{98}-Ab_2/Or_4-$Ab_{96,}$ an. 5 of Table 2 and an. 15 of Table 8) also occurs in the groundmass. Feldspar compositions are plotted in fig. 11 B. Fresh ferroaugite crystals of small dimensions were found only included in mesoperthite; otherwise they are completely replaced by a secondary yellowish and fibrous mineral (probably chlorite). Their composition, represented by Wo_{39-42}-En_{23-27}-Fs_{38-31} (an. 16-17 of Table 3 and fig. 6D), is in line with the high FeOtot/MgO value of the host rock (see Table 10).

The rare opaque minerals of all PAR are represented by magnetite (an. 6 and 8 of Table 7) and rare solid solutions of magnetite and ulvöspinel (TiO_2 up to 12.09 %, an. 7 of Table 7). The most common accessory phases are apatite and zircon, the latter particularly widespread, together with allanite, in ferroaugite displaying PAR, where large crystals (up to 2mm long) were observed. Fluorite is also present as an interstitial phase.

WHOLE ROCK CHEMISTRY AND PETROGENETIC CONSIDERATIONS

The chemical compositions of representative dyke rocks from NW Corsica are given in Table 10. Samples were selected trying to avoid high L.O.I values, normally linked to the development of secondary minerals rich in H_2O and CO_2. Besides propylitic alteration, extensive replacement of primary calcic plagioclase by secondary albite and K-feldspar, most probably related to autometasomatic processes, is also widespread in basaltic lithotypes. These reasons led us to focus geochemical examination on those elements generally considered to be poorly mobile during secondary processes, HFSE and REE (HREE and MREE), also taking into account, in basic and intermediate dykes, the composition of clinopyroxene, the best preserved mineral in their paragenesis.

Basaltic (AB, TrB, TchB, TchBA) and calc-alkaline dykes (BA, A)

AB and TrB represent evolved rocks (Mg*: 43÷52), as also confirmed by compatible elements such as Ni (47÷109 ppm) and Cr (58÷190 ppm). TchB and TchBA show SiO_2 contents (47.38% to 52.46%) higher than those of AB and TrB (43.77%-44.97%).

Among calc-alkaline dykes (SiO_2: 53.25%÷60.87%), only one BA (CB102) may be close to a primitive liquid, taking into account Mg* (65) and Cr contents (420 ppm), while the Ni value of 91 ppm testifies to fractionation of olivine. Considering its intergranular texture devoid of phenocrysts, we can assume that its primitive character is not linked to crystal accumulation.

Calc-alkaline and basaltic dykes are clearly distinguished in the AFM diagram (fig. 12), where FeOtot increases in the early stages of differentiation from AB to TchB, then drops through TchBA, and decreases from BA to A following a calc-alkaline trend. TiO_2 content is typically higher for basaltic dykes and increases in the same way as FeOtot, dropping through TchBA. Instead, calc-alkaline dykes, with the exception of sample CB130 (370 ppm), are characterized by higher Sr contents (627÷700 ppm) compared with basaltic ones (216÷389 ppm). K_2O content increases from BA to A, the former having a medium-K and the latter a high-K character. CaO, MgO and

TABLE 10

Major (wt%), trace elements (ppm), REE (ppm) contents and CIPW norms for NW Corsica dyke rocks.

	CB 12 AB	CB 16 AB	CB 89 TrB	CB 126 TrB	CB 21 TchB	CB 65 TchB	CB 66 TchB	CB 18 TchBA	CB 108 TchBA	CB 102 BA	CB 130 BA	CB 129 A	CB 120 A
SiO_2	44.97	44.32	44.79	43.77	49.08	48.27	47.38	51.63	52.46	53.25	53.94	57.55	60.87
TiO_2	2.90	2.16	2.25	1.87	1.88	2.60	2.78	2.29	1.48	1.06	1.41	1.04	1.02
Al_2O_3	15.35	15.97	15.20	16.30	15.48	13.90	14.09	15.07	15.89	13.75	17.06	15.99	16.26
Fe_2O_3	6.17	6.28	6.96	6.60	4.56	7.46	7.71	5.35	4.67	4.81	3.54	3.06	3.23
FeO	8.25	6.90	8.37	7.00	6.34	7.70	7.00	6.35	5.35	4.28	5.07	4.03	2.78
MnO	0.20	0.22	0.54	0.23	0.19	0.27	0.22	0.18	0.17	0.19	0.14	0.11	0.06
MgO	5.14	6.65	5.46	6.17	5.89	3.80	4.16	3.62	4.12	7.79	4.16	4.78	2.20
CaO	8.58	8.23	7.27	8.68	7.27	6.02	6.64	6.19	4.93	8.87	7.37	5.67	4.32
Na_2O	3.33	3.21	2.46	2.85	3.57	3.07	3.90	4.24	3.85	2.29	3.21	3.32	4.51
K_2O	1.04	1.03	1.42	0.54	2.48	2.17	1.43	2.19	2.86	1.37	1.70	2.49	2.89
P_2O_5	0.70	0.64	0.53	0.65	0.34	1.29	1.32	0.36	0.50	0.25	0.31	0.27	0.42
H_2O+	3.38	4.41	4.75	5.35	2.93	3.46	3.38	2.55	3.72	2.10	2.10	1.69	1.45
Total	100.00	100.00	100.00	100.00	100.00	100.00	100.00	100.00	100.00	100.00	100.00	100.00	100.00
V	307	215	258	222	208	234	300	235	168	190	119	126	102
Cr	58	190	88	93	100	11	12	67	45	419	20	224	65
Co	41	43	39	46	27	18	24	27	26	31	26	23	13
Ni	47	109	53	83	40	28	31	34	52	91	31	108	46
Zn	138	127	146	136	156	146	142	124	132	129	89	107	42
Rb	40	94	152	24	98	134	57	80	164	119	82	154	228
Sr	341	371	389	251	222	338	290	216	285	642	370	627	662
Ba	385	173	447	178	370	803	638	498	482	333	240	755	788
Pb	6	14	27	6	13	6	3	9	30	15	6	15	5
Nb	15	14	11	9	11	16	23	18	10	6	6	13	20
Zr	303	268	296	196	285	324	341	299	279	160	211	200	272
Th	3	9	4	2	7	6	7	5	3	4	8	11	16
Y	37	38	58	23	42	65	55	45	58	34	31	42	55
La	21.90	20.00	20.80	15.47	24.20	26.44	35.30	25.50	26.10	14.10	18.60	28.30	50.00
Ce	57.00	52.00	54.00	47.77	60.00	70.18	93.00	65.00	64.00	33.50	45.00	62.00	102.00
Pr	7.36	6.68	6.93	n.d.	7.07	n.d.	11.60	8.05	7.87	4.10	5.18	6.59	11.00
Nd	34.60	31.80	34.60	n.d.	32.40	n.d.	57.80	37.60	35.80	19.10	22.60	27.60	45.20
Sm	7.86	6.93	8.03	n.d.	7.11	n.d.	13.00	8.39	7.64	3.96	5.17	5.60	7.55
Eu	2.71	2.28	2.51	n.d.	1.82	n.d.	4.54	2.04	2.13	1.18	1.64	1.47	1.90
Gd	8.92	7.62	8.60	n.d.	7.27	n.d.	13.20	8.91	8.17	4.18	5.21	4.68	6.73
Tb	1.39	1.17	1.43	n.d.	1.15	n.d.	2.07	1.46	1.30	0.66	0.83	0.70	0.86
Dy	7.54	6.28	8.16	n.d.	6.75	n.d.	11.60	8.25	7.01	3.73	4.73	3.95	4.16
Ho	1.62	1.33	1.67	n.d.	1.45	n.d.	2.33	1.71	1.47	0.79	0.98	0.79	0.81
Er	4.64	3.79	4.79	n.d.	4.02	n.d.	6.49	5.07	4.29	2.32	2.71	2.18	2.27
Tm	0.64	0.52	0.71	n.d.	0.59	n.d.	0.93	0.74	0.61	0.34	0.39	0.32	0.31
Yb	3.99	3.22	4.43	n.d.	3.85	n.d.	5.91	4.56	3.64	2.15	2.48	2.06	1.89
Lu	0.61	0.50	0.65	n.d.	0.60	n.d.	0.84	0.71	0.58	0.32	0.37	0.31	0.26
Hf	6.20	5.20	6.20	n.d.	6.30	n.d.	8.10	7.10	6.90	3.00	4.30	4.30	6.30
Ta	1.00	0.90	0.70	n.d.	0.80	n.d.	1.20	1.30	0.90	0.50	0.70	0.80	1.10
REEsum	160.78	144.12	157.31		158.28		258.61	177.99	170.61	90.43	115.89	146.55	234.94
$(La/Yb)_n$	3.7	4.2	3.2		4.3		4.0	3.8	4.9	4.4	5.1	9.3	17.9
Eu/Eu*	0.99	0.96	0.92		0.77		1.05	0.72	0.82	0.88	0.96	0.85	0.80
CIPW Norms (wt%)													
Q										3.63	4.55	7.26	9.67
C													
Or	6.15	6.09	8.40	3.19	14.63	12.80	8.45	12.93	16.91	8.10	10.04	14.72	17.10
Ab	26.35	23.81	20.79	24.08	26.92	26.00	32.97	35.89	32.55	19.39	27.12	28.13	38.18
An	23.86	26.11	26.26	30.10	18.93	17.75	16.73	15.61	17.64	23.17	27.15	21.35	15.56
Ne	0.99	1.82			1.76								
Ac													
Ns													
Di	11.80	8.71	5.28	7.24	12.27	3.13	6.42	10.69	2.97	15.63	6.11	4.13	2.63
Hy			12.42	3.40		25.03	10.22	7.65	17.26	23.38	17.71	18.61	11.18
Ol	17.27	20.61	13.28	18.61	15.88	0.60	10.25	6.99	2.81				
Hm													
Mt	2.64	2.40	2.80	2.48	2.00	2.76	2.67	2.14	1.83	1.65	1.58		
Ilm	5.50	4.10	4.27	3.56	3.57	4.93	5.28	4.34	2.81	2.02	2.68	1.30	1.09
Hap	1.64	1.51	1.26	1.54	0.81	3.03	3.10	0.85	1.18	0.58	0.73	1.97	1.93
H2O+	3.35	4.38	4.73	5.32	2.92	3.40	3.32	2.53	3.70	2.08	2.09	0.63	0.98
Total	99.56	99.54	99.50	99.51	99.68	99.44	99.41	99.61	99.66	99.63	99.75	1.68	1.43
Mg*	42.96	51.73	43.01	49.09	53.29	34.78	37.63	39.61	46.59	64.65	50.47	58.75	43.90
A/CNK	0.75	0.81	0.87	0.84	0.74	0.91	0.83	0.76	0.92	0.66	0.86	0.90	0.93
A.I.	0.43	0.40	0.37	0.32	0.55	0.53	0.56	0.62	0.59	0.38	0.42	0.51	0.65
Y/Nb	2.50	2.73	5.29	2.58	3.89	4.08	2.39	2.47	5.91	6.03	4.78	3.25	2.81

TABLE 10: *Continued*

	CB 97 A	CB 25 PAR	CB 26 PAR	CB 27 PAR	CB 30 PAR	CB 105 PAR	CB 100 PAR	CB 64 R	CB109 R	CB 110 R	CB 112 R	CB 95 R	CB 96 R
SiO_2	59.22	74.38	74.71	73.68	74.62	74.02	71.48	77.81	73.60	75.64	77.32	75.72	76.38
TiO_2	0.93	0.13	0.15	0.17	0.12	0.22	0.26	0.11	0.18	0.17	0.12	0.04	0.10
Al_2O_3	16.01	11.59	11.47	11.49	11.80	10.78	13.76	11.91	12.45	11.41	11.53	13.47	13.08
Fe_2O_3	4.55	2.73	3.08	3.03	2.64	3.23	1.87	1.29	2.99	2.92	1.23	0.07	0.29
FeO	2.90	1.39	1.20	1.59	1.25	2.16	0.96	0.38	1.52	0.46	0.45	0.25	0.24
MnO	0.12	0.06	0.06	0.07	0.05	0.09	0.06	0.03	0.03	0.03	0.04	0.03	0.03
MgO	2.91	0.25	0.25	0.23	0.17	0.28	0.29	0.35	1.15	0.82	0.56	0.29	0.25
CaO	4.27	0.16	0.11	0.62	0.09	0.13	0.49	0.12	0.03	0.03	0.02	0.79	0.71
Na_2O	4.33	4.77	4.53	4.69	4.80	4.25	4.29	3.38	1.80	3.25	3.34	3.72	3.73
K_2O	1.93	3.95	3.98	3.93	3.93	4.03	5.45	3.41	4.62	4.28	4.59	5.13	4.67
P_2O_5	0.36	0.00	0.00	0.01	0.00	0.02	0.04	0.01	0.00	0.00	0.00	0.02	0.01
H_2O+	2.47	0.59	0.46	0.51	0.52	0.78	1.07	1.22	1.64	1.00	0.80	0.47	0.52
Total	100.00	100.00	100.00	100.00	100.00	100.00	100.00	100.00	100.00	100.00	100.00	100.00	100.00
V	97	3	4	4	2	4	7	8	6	4	3	3	7
Cr	10	2	5	1	3	1	1	7	4	5	3	7	4
Co	13	3	0	4	0	3	0	2	2	1	2	2	0
Ni	26	31	31	40	26	28	23	25	25	27	25	22	24
Zn	90	340	316	477	307	238	93	36	46	45	14	4	5
Rb	83	550	499	749	489	253	125	154	187	193	223	292	206
Sr	699	5	2	16	1	1	21	18	1	5	6	148	89
Ba	621	117	120	200	101	156	268	240	116	106	107	340	174
Pb	10	25	84	176	17	41	20	7	6	5	3	43	36
Nb	13	97	140	149	120	103	27	41	74	82	45	5	5
Zr	247	1906	2074	3346	1521	1688	641	529	1491	1666	673	45	73
Th	6	83	92	139	96	35	18	31	44	47	31	20	40
Y	32	275	325	717	150	195	62	86	167	160	107	54	38
La	24.49	80.91	137.00	184.00	65.08	109.00	101.00	27.12	70.45	70.70	60.18	16.08	19.90
Ce	42.79	215.44	270.00	481.00	180.07	282.00	223.00	56.53	205.14	184.00	140.85	5.16	42.00
Pr	n.d.	n.d.	47.40	58.40	n.d.	31.80	23.90	n.d.	n.d.	22.10	n.d.	n.d.	4.00
Nd	n.d.	n.d.	199.00	260.00	n.d.	135.00	96.20	n.d.	n.d.	94.90	n.d.	n.d.	13.70
Sm	n.d.	n.d.	52.40	68.10	n.d.	29.90	15.50	n.d.	n.d.	23.40	n.d.	n.d.	2.00
Eu	n.d.	n.d.	1.97	2.52	n.d.	1.47	0.59	n.d.	n.d.	0.51	n.d.	n.d.	0.43
Gd	n.d.	n.d.	53.30	75.40	n.d.	29.30	13.40	n.d.	n.d.	23.20	n.d.	n.d.	1.48
Tb	n.d.	n.d.	9.17	14.80	n.d.	5.31	1.92	n.d.	n.d.	4.19	n.d.	n.d.	0.16
Dy	n.d.	n.d.	52.40	90.50	n.d.	33.20	9.85	n.d.	n.d.	27.20	n.d.	n.d.	0.78
Ho	n.d.	n.d.	10.70	19.40	n.d.	7.12	1.98	n.d.	n.d.	6.18	n.d.	n.d.	0.15
Er	n.d.	n.d.	29.90	57.70	n.d.	21.10	5.84	n.d.	n.d.	18.30	n.d.	n.d.	0.46
Tm	n.d.	n.d.	4.57	9.15	n.d.	3.29	0.92	n.d.	n.d.	2.81	n.d.	n.d.	0.07
Yb	n.d.	n.d.	28.80	54.10	n.d.	21.50	5.68	n.d.	n.d.	17.20	n.d.	n.d.	0.54
Lu	n.d.	n.d.	4.28	7.61	n.d.	3.25	0.89	n.d.	n.d.	2.61	n.d.	n.d.	0.11
Hf	n.d.	n.d.	54.00	93.00	n.d.	37.00	14.00	n.d.	n.d.	36.00	n.d.	n.d.	3.10
Ta	n.d.	n.d.	11.00	16.00	n.d.	5.30	1.50	n.d.	n.d.	4.90	n.d.	n.d.	0.70
REE			900.89	1382.78		713.24	500.67			497.30			85.78
$(La/Yb)_n$			3.2	2.3		3.4	12.0			2.8			25.0
Eu/Eu*			0.11	0.11		0.15	0.12			0.07			0.73
CIPW Norms (wt%)													
Q	10.02	31.20	32.96	30.53	31.50	33.16	24.32	44.37	40.92	39.07	39.45	32.22	34.90
C							0.01	2.46	4.44	1.37	1.04	0.41	0.62
Or	11.41	23.35	23.52	23.20	23.25	23.83	32.22	20.14	27.29	25.28	27.13	30.32	27.61
Ab	36.64	37.63	36.83	37.22	38.80	32.99	36.26	28.56	15.19	27.53	28.26	31.45	31.57
An	18.56						2.17	0.56	0.14	0.14	0.08	3.80	3.44
Ne													
Ac		2.42	1.35	2.19	1.62	2.63							
Ns													
Di	0.24	0.64	0.44	2.53	0.33	0.46							
Hy	16.37	1.18	0.42	0.20	0.73	2.32	0.72	0.87	8.98	2.04	1.39	1.10	0.72
Ol													
Hm			0.11				0.11	0.61		2.17	0.38		
Mt	1.34	2.74	3.62	3.30	3.02	3.37	2.54	0.98	0.81	1.09	1.23	0.11	0.42
Ilm	1.76	0.25	0.28	0.32	0.23	0.42	0.49	0.22	0.34	0.31	0.23	0.08	0.18
Hap	0.85	0.00		0.01	0.01	0.04	0.09	0.01		0.00	0.00	0.05	0.03
H_2O+	2.46	0.00	99.53	0.00	0.00	0.00	0.00	0.00	1.64	0.00	0.00	0.00	0.00
Total	99.64	99.41			99.49			98.78	99.76	99.00	99.19	99.54	99.49
Mg*	45.49	11.62	11.30	9.72	8.66	10.05	18.18	31.51	35.58	34.95	42.12	65.01	50.27
A/CNK	0.99	0.93	0.96	0.88	0.96	0.93	1.00	1.26	1.56	1.14	1.10	1.03	1.02
A.I.	0.58	1.05	1.03	1.04	1.03	1.05	0.94	1.78	0.64	0.87	0.91	0.87	0.86
Y/Nb	2.39	2.84	2.32	4.80	1.25	1.89	2.30	2.07	2.25	1.95	2.38	10.20	7.59

TABLE 10: *Continued*

	CB 55 R	CB 81 R	CB 72 R	CB 61 PR	CB 68 PR	CB 70 PR
SiO_2	75.52	70.79	72.81	71.98	72.81	71.58
TiO_2	0.07	0.33	0.18	0.17	0.06	0.18
Al_2O_3	12.95	14.93	14.58	15.14	15.34	15.44
Fe_2O_3	0.94	3.00	0.64	0.68	0.68	0.88
FeO	0.36	0.33	0.25	0.30	0.27	0.42
MnO	0.03	0.06	0.03	0.04	0.04	0.04
MgO	0.19	0.92	0.34	0.52	0.30	0.46
CaO	0.36	0.28	0.67	0.33	0.34	0.91
Na_2O	3.64	3.44	3.66	3.82	4.20	3.92
K_2O	4.80	4.03	5.55	5.73	4.68	5.12
P_2O_5	0.01	0.12	0.05	0.18	0.19	0.10
H_2O+	1.12	1.77	1.24	1.12	1.09	0.97
Total	100.00	100.00	100.00	100.00	100.00	100.00
V	2	40	11	9	4	11
Cr	5	6	3	5	4	7
Co	2	10	2	2	0	2
Ni	26	23	23	25	23	24
Zn	28	36	9	12	15	18
Rb	298	163	270	178	241	224
Sr	15	112	168	227	94	213
Ba	68	531	608	1177	149	513
Pb	8	11	49	35	30	54
Nb	40	13	15	1	10	8
Zr	116	110	106	194	29	84
Th	29	16	38	30	7	13
Y	118	46	61	42	49	46
La	12.03	24.7	49.30	43.89	3.33	17.90
Ce	33.06	53.0	107.00	80.73	7.70	38.00
Pr	n.d.	5.7	10.80	n.d.	0.85	3.98
Nd	n.d.	22.6	38.10	n.d.	3.29	15.80
Sm	n.d.	4.4	6.27	n.d.	0.98	3.43
Eu	n.d.	0.6	0.62	n.d.	0.17	0.92
Gd	n.d.	4.2	4.99	n.d.	1.10	2.91
Tb	n.d.	0.7	0.62	n.d.	0.22	0.42
Dy	n.d.	3.9	3.01	n.d.	1.43	2.03
Ho	n.d.	0.8	0.58	n.d.	0.29	0.33
E	n.d.	2.5	1.65	n.d.	0.82	0.86
Tm	n.d.	0.4	0.24	n.d.	0.13	0.13
Yb	n.d.	2.6	1.55	n.d.	0.83	0.77
Lu	n.d.	0.4	0.23	n.d.	0.13	0.10
Hf	n.d.	3.2	3.70	n.d.	1.00	2.20
Ta	n.d.	1.7	1.80	n.d.	2.10	1.10
REE		126.48	224.96		21.27	87.58
$(La/Yb)_n$		6.4	21.5		2.7	15.7
Eu/Eu*		0.39	0.33		0.50	0.87
CIPW Norms (wt%)						
Q	34.93	33.74	28.49	26.87	29.82	26.82
C	1.13	4.70	1.46	2.49	3.19	2.03
Or	28.37	23.84	32.80	33.84	27.63	30.26
Ab	30.82	29.10	30.95	32.32	35.56	33.17
An	1.73	0.56	2.98	0.46	0.47	3.86
Ne						
Ac						
Ns						
Di						
Hy	0.47	2.29	0.85	1.30	0.75	1.15
Ol						
Hm	0.20	2.78	0.38	0.27	0.11	0.20
Mt	1.08	0.32	0.38	0.60	0.83	0.97
Ilm	0.13	0.62	0.35	0.32	0.11	0.33
Hap	0.03	0.29	0.13	0.42	0.45	0.23
H_2O+	0.00	-0.01	0.00	-0.01	-0.01	0.00
Total	98.89	98.23	98.77	98.88	98.91	99.02
Mg*	24.16	38.06	45.45	53.53	40.78	43.50
A/CNK	1.10	1.46	1.11	1.20	1.26	1.15
A.I.	0.86	0.67	0.82	0.82	0.78	0.78
Y/Nb	2.99	3.39	4.04	29.99	5.13	5.70

AB: alkali basalt; TrB: transitional basalt; TchB: trachybasalt; TchBA: basaltic-trachyandesite; BA: basaltic-andesite; A: andesite; R: biotitic rhyolite; PAR: peralkaline rhyolite; PR: peraluminous rhyolite. C.I.P.W. norm, except for rhyolitic rocks, calculated on normalized ratio $Fe_2O_3/FeO=0,15$; Mg* corrected for normalized ratio $Fe_2O_3/FeO=0,15$; $A/CNK=Al_2O_3/(CaO+Na_2O+K_2O-10/3*P_2O_5)$ mol.; $A.I.=(K_2O+Na_2O)/Al_2O_3$mol; Eu/Eu*: Eu anomaly.

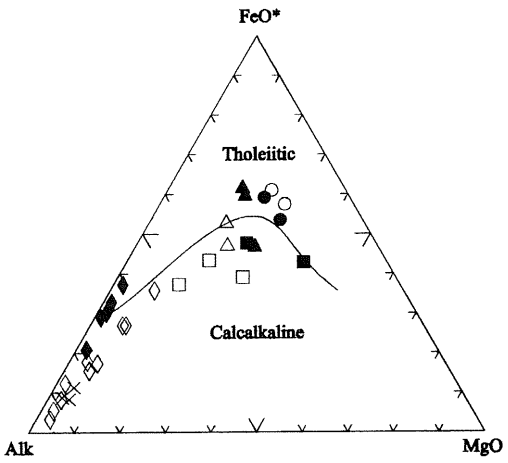

Fig. 12 - Alk-FeO*-MgO diagram for NW Corsica dyke rocks. Alk: Na_2O+K_2O; FeO*: FeO_{tot}. Tholeiitic-calcalkaline field separation line according to Irvine and Baragar (1971). Symbols as in fig. 3.

compatible elements (e.g.: Co, Cr, Ni) decrease with differentiation in both calc-alkaline and basaltic dykes, suggesting olivine and clinopyroxene fractionation.

Mass balance calculations for basaltic dykes indicate that TchB (represented by sample CB21) may have generated by 51% fractional crystallization of a mineral assemblage consisting of olivine (30.6%), labradorite plagioclase (57.4%), augite clinopyroxene (4.7%), ilmenite (5.0%) and apatite (2.3%), starting from AB magma (represented by the less evolved sample CB16, Table 10). TchB in turn gave rise to TchBA (CB108) by removal of 35% of a mineral assemblage represented by olivine (19.6%), labradorite plagioclase (45.9%), augite clinopyroxene (27.5%), magnetite (1.6%) and ilmenite (5.4%).

Major elements were modeled using the XL-FRAC calculation program (Stormer and Nicholls, 1978) which provides a least-squares fit to data based on ten major oxides; results were subsequently tested for trace elements using the Rayleigh fractionation model. Results are presented in Table 11; crystal/liquid partition coefficients for trace elements are taken from the literature and reported in Table 12. As regards olivine and plagioclase compositions, analyses taken from other late Hercynian dykes in Sardinia were used (Traversa, unpublished) since these minerals are completely replaced in NW Corsica basaltic dykes.

Trace element modeling is fully satisfactory except for Rb and Zr. Rb calculated values are higher than the observed ones in the fractionation from CB16 to CB21, and lower in the transition from CB21 to CB108. The latter feature may be explained by crustal contamination affecting CB108 liquid during its ascent, since simple fractional crystallization cannot account for such Rb enrichment, although the lowest partition coefficients from the literature were used for modeling; however, the lower observed values for Zr relative to those calculated for CB108 do not support this hypothesis (Tab.11). Conversely, the lower Rb contents of CB21 relative to those calculated may indicate crustal contamination of the presumed parent magma CB16 (discussed later).

On the MORB-normalized spidergrams (fig. 13), all basaltic dykes show broadly comparable trends, characterized by enrichment of LILE and Th with respect to HFSE. More compatible elements Y and Yb are close to one and Cr is depleted. Only sample CB66 (TchB) differs from the other evolved basaltic dykes in that it is more enriched in P and Ce, due to the high content of apatite of the rock. Slight Nb and Ta enrichment with respect to MORB (less than 10 times) are not typical of alkaline magmas, which are usually referred to an enriched magma source (E-MORB), but rather of magmas which erupted in subduction-related tectonic settings. LILE enrichment, related to mantle metasomatism operated by hydrous fluids deriving from dehydration of a subducting slab in arcs (Hawkesworth *et al.*, 1993; Poli and Schimdt, 1995) may, in this case, refer to the breakdown of hydrous phases present in the mechanical boundary layer in the subcontinental mantle (Gallagher and Hawkesworth, 1992) or to the presence of

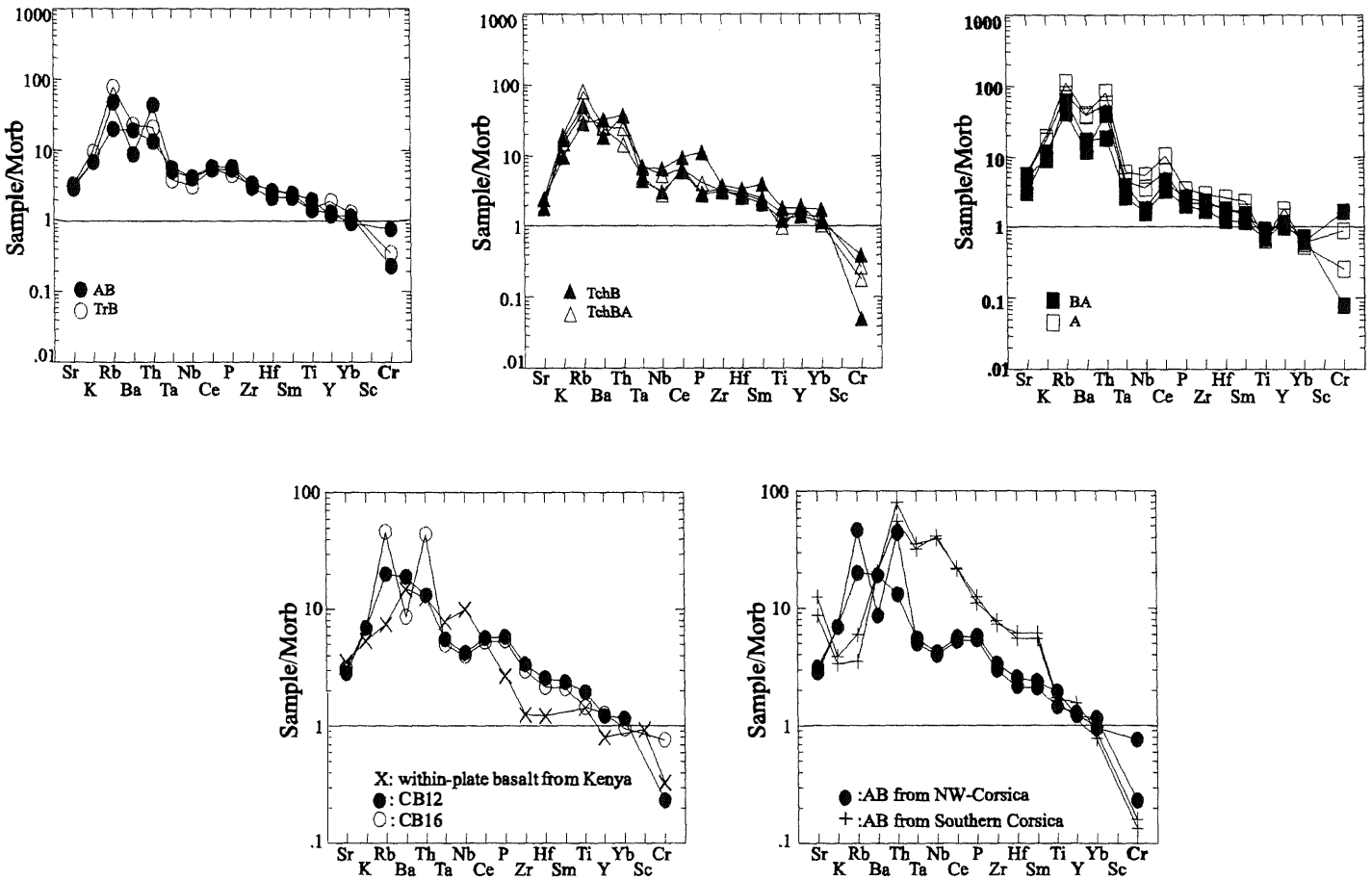

Fig. 13 - MORB-normalized trace element patterns for some representative basaltic and calc-alkaline NW Corsica dyke rocks. Normalizing values from Pearce (1982). Abbreviations as in fig. 3.

TABLE 11

Major and trace element mass-balance calculations of fractional crystallization model for NW Corsica basic dykes.

	From CB16 AB to CB21 TchB			From CB21 TchB to CB108 TchBA		
	obs	calc	obs	obs	calc	obs
SiO_2	46.66	50.75	50.8	50.8	54.39	54.75
TiO_2	2.27	1.94	1.95	1.95	1.32	1.54
Al_2O_3	16.81	15.96	16.02	16.02	16.46	16.58
FeO_{tot}	13.21	10.75	10.81	10.81	9.76	9.97
MnO	0.23	0.16	0.2	0.2	0.12	0.18
MgO	7	6.14	6.1	6.1	4.26	4.3
CaO	8.66	7.49	7.52	7.52	5.15	5.15
Na_2O	3.38	4.08	3.69	3.69	4.41	4.02
K_2O	1.08	2.36	2.57	2.57	3.60	2.99
P_2O_5	0.67	0.31	0.35	0.35	0.53	0.52
R^2	0.21			0.75		
% F	49.37			65.23		
Olivine% [a]	30.59	Fo_{64}-Fa_{36} [b]		19.63	Fo_{50}-Fa_{50} [b]	
Pyroxene% [a]	4.69	Wo_{45}-En_{37}-Fs_{18}		27.52	Wo_{45}-En_{37}-Fs_{18}	
Plagioclase% [a]	57.4	An_{64}-Ab_{36} [b]		45.86	An_{64}-Ab_{36} [b]	
Apatite% [a]	2.32			—		
Magnetite% [a]	—			1.56		
Ilmenite% [a]	5.0			5.44		

	From CB16 AB to CB21 TchB				From CB21 TchB to CB108 TchBA			
	obs	calc	obs	D	obs	calc	obs	D
Rb	94	163	98	0.23	98	140	164	0.01
Ba	173	348	370	0.03	370	487	482	0.32
Sr	371	227	222	1.73	222	283	285	0.50
V	215	257	208	1.03	208	166	168	1.55
Cr	190	98	100	1.89	100	44	44	2.95
Ni	109	40	40	2.41	40	1	1	9.33
Zr	268	434	285	0.28	285	327	280	0.68
Y	38	50	42	0.57	42	58	58	0.23
La	20	24.1	24.2	0.67	24.2	30.6	26.1	0.47
Ce	52	61.5	60	0.68	60	69.9	64	0.43
Yb	3.2	4.8	3.8	0.45	3.8	4.6	3.64	0.44

[a]: wt% of mineral removed during fractionation; [b]: compositions of olivine and plagioclase from Northern Sardinia late-Hercynian basaltic dykes (Traversa, unpublished); R^2: sum of residual squares; %F: wt% of residual liquid.

ancient subducted crust. The positive Pb spike (fig. 14) of AB and TrB is another character recalling calc-alkaline affinity, but it is probably related to crustal contamination undergone by these basaltic dykes during their ascent to the surface.

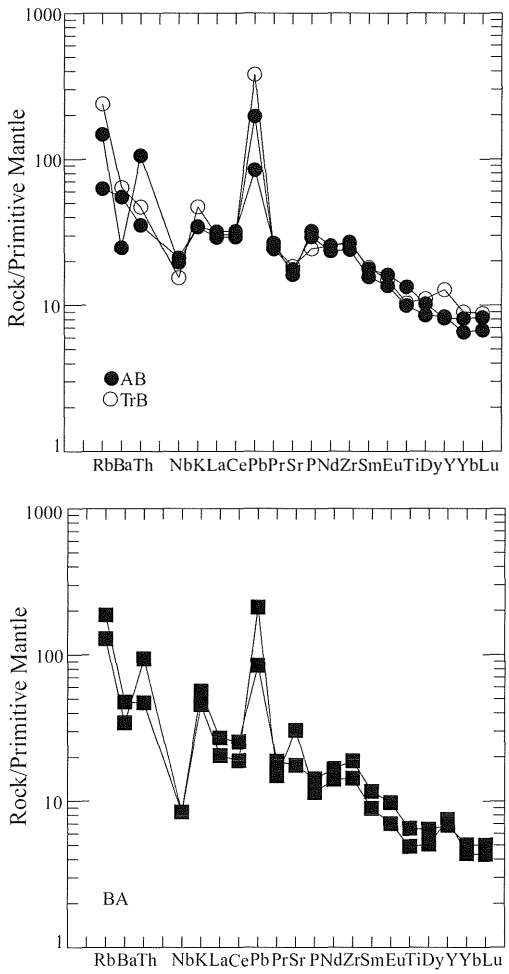

Fig. l4 - Primitive Mantle (P.M.) normalized spidergrams for some representative basaltic and calc-alkaline NW Corsica dyke rocks. Normalizing values from Sun and McDonough (1989). Abbreviations as in fig. 3.

Nevertheless, comparison between AB and an intracontinental alkali basalt (Kenya Rift, Baker *et al.,* 1977) (fig. 13) shows similar trends on the whole, but the well-marked Nb trough of AB confirms derivation of these liquids from a subcontinental mantle with depleted composition. Moreover, the extreme enrichment in Rb and Th for sample CB16 (fig. 13), together with positive Pb spikes, are further indications of crustal contamination. In this regard, Sr-Nd isotopic determinations are in progress.

Compared with alkali basaltic dykes from Southern Corsica (fig. 13), AB show strong depletion in Ta and Nb and generally in all elements from Ta to Sm. As regards LILE, they are particularly enriched in Rb and depleted in Sr. This highlights a difference in the magma source for alkali basalts from southern and northern Corsica, confirming the depleted nature of the mantle source, together with crustal contamination, for the latter. Accordingly, the Sr-Nd initial isotope ratio for southern Corsica ($^{87}Sr/^{86}Sr_{280}$=0.70388÷0.70412, $^{143}Nd/^{144}Nd_{280}$=0.512550÷0.512561, Pasquali, 1998) demonstrates the almost complete lack of crustal contamination processes.

BA trends on MORB-normalized spidergrams (fig. 13) are characteristic of calc-alkaline basalts from volcanic arc settings as regards their LILE enrichment but not of HFSE ones, which are usually depleted in such magmas; Th, Ce and P contents match the medium/high-K character of BA and A (Pearce, 1982). HFSE enrichment may be related to either mantle source metasomatism or mixing of magmas from two separate sources. The positive Pb spike shown by BA (fig. 14) supports crustal contamination, possibly operated by ancient sedimentary subducted material, as already discussed for basaltic dykes.

The ΣREE of basaltic dykes is quite modest (144÷178 ppm), rising only in sample CB66 (ΣREE: 259 ppm), and LREE/HREE fractionation is low (La_n/Yb_n: 3.2÷4.9), even in the more evolved litotypes like TchBA. The negative Eu anomaly is, on the whole, not greatly marked and even completely lacking in sample CB66 (Table 10). These patterns (fig. 15) are not typical of basic alkaline melts derived from an undepleted mantle source, but it does testify once again to depletion of the source. In confirmation, northern Sardinia late Hercynian alkaline basic dykes show higher LREE contents (up to 200 times chondritic values), and their low Sr_i isotopic values

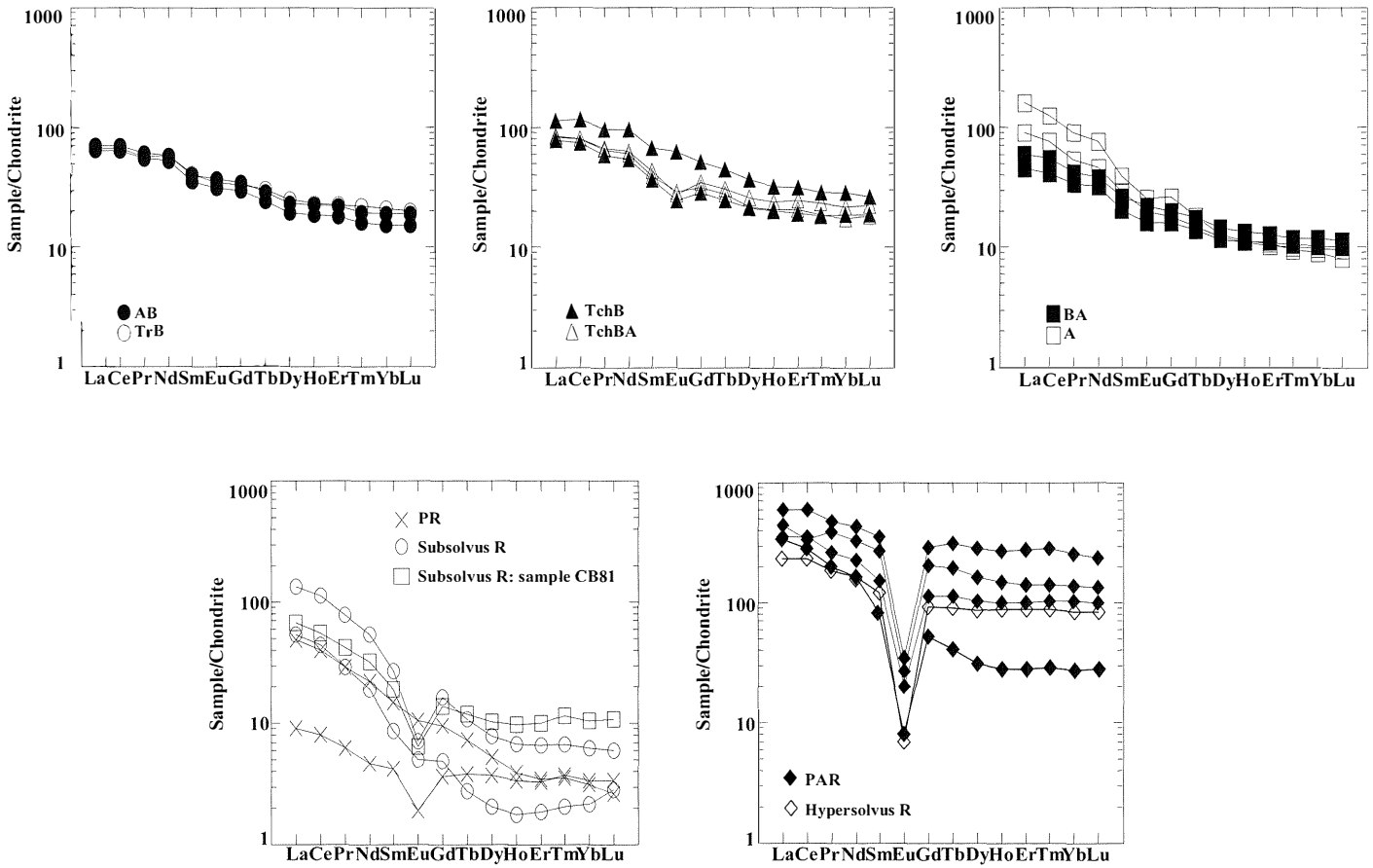

Fig. 15 - Chondrite-normalized REE patterns for some representative NW Corsica dyke rocks. Normalizing values from Boynton (1984). Abbreviations as in fig. 3

TABLE 12

Trace element crystal/liquid partition coefficients for fractional crystallization modeling.

	Plagioclase		Clinopyroxene		Olivine		Apatite		Magnetite		Ilmenite	
	from CB16 to CB21	from CB21 to CB108	from CB16 to CB21	from CB21 to CB108	from CB16 to CB21	from CB21 to CB108	from CB16 to CB21	from CB21 to CB108	from CB16 to CB21	from CB21 to CB108	from CB16 to CB21	from CB21 to CB108
Rb	0.3	0.01	0.13	0.01	0.08	0.01	0.01	—	—	0.11	0.47	0.01
Ba	0.05	0.6	0.001	0.01	0.001	0.1	0.01	—	—	0.01	0.01	0.01
Sr	2.8	1.04	0.07	0.05	0.01	0.01	5	—	—	0.01	0.01	0.01
V	0.1	0.1	3.1	3.1	0.09	0.09	0.01	—	—	0.1	12	12
Cr	0.08	0.08	8	3.8	3.8	5	0.04	—	—	35	6	6
Ni	0.06	0.06	4.4	5	6.8	34	0.01	—	—	60	1.8	3.5
Zr	0.27	0.27	0.004	1.02	0.12	0.66	3	—	—	8	0.4	0.4
Y	0.03	0.03	1.05	0.7	0.12	0.12	20	—	—	0.17	0.15	0.1
La	0.24	0.32	0.4	0.66	0.1	0.4	20	—	—	2.9	0.39	0.39
Ce	0.24	0.24	0.18	1.05	0.01	0.01	23	—	—	0.34	0.1	0.6
Yb	0.08	0.1	1.01	1.05	0.39	0.35	9	—	—	0.4	0.7	0.7

References: Bougault and Hekinian (1974); Le Roex and Herlank (1982); Lemarchand *et al.* (1987); Villemant *et al.* (1981).

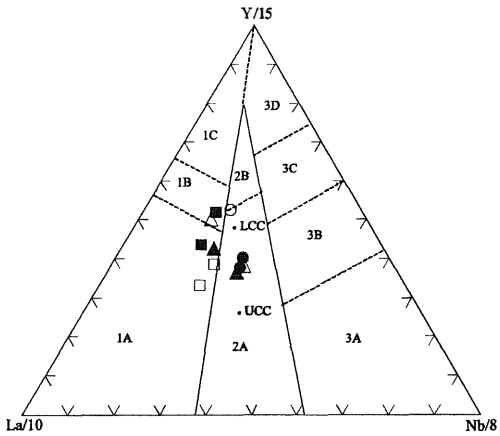

Fig. 16 - Y/15-La/10-Nb/8 tectonic discrimination diagram (after Cabanis and Lecolle, 1989) for basaltic and calc-alkaline NW Corsica dyke rocks. Symbols as in fig. 3. 1 = orogenic domain (volcanic arc basalts) 1A: calc-alkaline basalts; 1C: volcanic arc tholeiites; 1B: area overlapping 1A and 1C. 2 = late- to post-orogenic intra-continental domain 2A: continental basalt; 2B: back-arc basin basalt. 3 = anorogenic domain 3A: alkali basalt from intercontinental rift; 3B: E-MORB; 3C: weakly enriched MORB; 3D: N-MORB. LCC: lower continental crust. UCC: upper continental crust.

(0.70389±0.00041, Traversa and Vaccaro, 1992) support derivation from an undepleted astenospheric source.

BA show lower REE enrichment and slightly higher LREE/HREE fractionation relative to AB and TrB (ΣREE: 90÷116 ppm, La_n/Yb_n 4.4÷5.1). The ΣREE value of 90 ppm for sample CB102 (BA) is further proof of its primitive character, as highlighted before. ΣREE and LREE/HREE fractionation increases in A (La_n/Yb_n: 9.3÷17.9, ΣREE: 146÷235 ppm, see fig. 15), LREE ranging from 100 to around 200 times chondritic values. The negative Eu anomaly also increases with differentiation, but not as much as for the more evolved basaltic dykes (TchBA), indicating the lack of a genetic link between BA and A, as also revealed by their respective medium- and higk-K characters and confirmed by mass balance calculations.

As regards the relation between tectonic settings and magma compositions for NW Corsica basaltic and calcalkaline dykes, the La/10-Y/15-Nb/8 diagram of Cabanis and Lecolle (1989, fig. 16) is well discriminating in

this regard. AB and TrB plot in the post-orogenic intra-continental domain, spanning lower and upper continental crust compositions. Such a crustal signature, already mentioned on the basis of LILE enrichment, may either indicate crustal assimilation undergone by basaltic magma during its ascent or a subduction-modified mantle source component involved in its genesis. Clearly, basaltic dyke magmatism from NW Corsica cannot be referred to an uncontaminated astenospheric mantle source, as previously believed, on the basis of isotopic Sr and Nd data, for the northern Sardinia and southern Corsica basaltic alkaline phase (Vaccaro *et al.,* 1991; Traversa and Vaccaro, 1992; Pasquali and Traversa, 1996; Pasquali, 1998). Rather, its geodynamic setting refers to a post-collisional domain, predating a true rift-related tectonic setting in which anorogenic mantle prevailed. Presumed crustal contamination may be related to regions with high rates of crustal extension, as they are associated with higher magma production rates inducing higher geothermal gradients in the crust. This would support an already extensional post-collisional environment in which the NW Corsica alkali basaltic dyke magmatism can be placed. Instead, the calc-alkaline dykes plotted in fig. 16 fall in the orogenic domain and are probably to be attributed to a phase preceding the alkaline one, although there is no crosscutting evidence in the field.

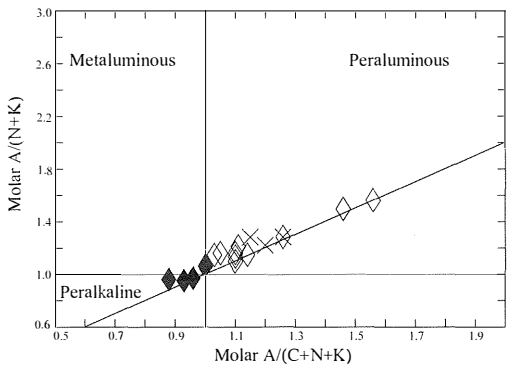

Fig. 17 - Distribution of NW Corsica rhyolitic dyke rocks in A/(N+K) and A/(C+N+K) space (Shand's index, after Maniar and Piccoli, 1989). Symbols as in fig. 3.

Rhyolitic dykes (PR, PAR, R)

Taking into account Shand's index (fig. 17) and CIPW normative minerals (Tab. 10), PR and R may be regarded as metaluminous to peraluminous (A/CNK:1.03÷1.56, normative Corundum: 0.41÷4.7) and PAR as peralkaline (A/NK: 0.95÷0.97, normative Acmite: 1.35÷2.63), except for the few metaluminous ones.

The strong peraluminous character of some R is the consequence of alkali loss due to subsolidus processes, often accompanied by reddening of the lithotype (Egeberg *et al.,* 1993), since no primary peraluminous minerals (e.g.: muscovite, garnet, etc.) were detected in these rocks. Moreover, R are generally characterized by low Na_2O contents (fig. 18) compared with PAR and PR.

Selected major and trace elements *vs.* SiO_2 diagrams (figs. 18, 19) clearly summarize the main geochemical differences between the various rhyolitic dykes. In fig. 18, PAR, with the exception of samples with ferroaugite clinopyroxene, plot as a cluster of points, indicating quite constant internal composition, while R are scattered. All rhyolitic dykes are characterized by very low compatible trace element contents (e.g.: Cr, Co, V), except for Ni (fig. 19); moreover, the highest Zn contents for PAR discriminate them from PR and R (fig. 19) and identify these dykes as the «paisanites» (Quin, 1968) outcropping in the same area (Bonin, 1988; Egeberg *et al.*, 1993).

PAR are represented by rocks of comparable degree of evolution (SiO_2: 72%-75%). Salient chemical features are the constant fairly high alkali contents (8.3%÷9.7%), low MgO, CaO, Sr, high FeOtot and Na_2O, and a higher FeOtot/MgO value compared with the other rhyolitic dykes (see Table 10). These features, together with enhanced levels of Nb, Zr, Y, Ga and REE (except Eu) and the Rb/Sr ratio, point to the affinity of PAR with A-type granites (Whalen *et al.,* 1987; Eby, 1990), as confirmed

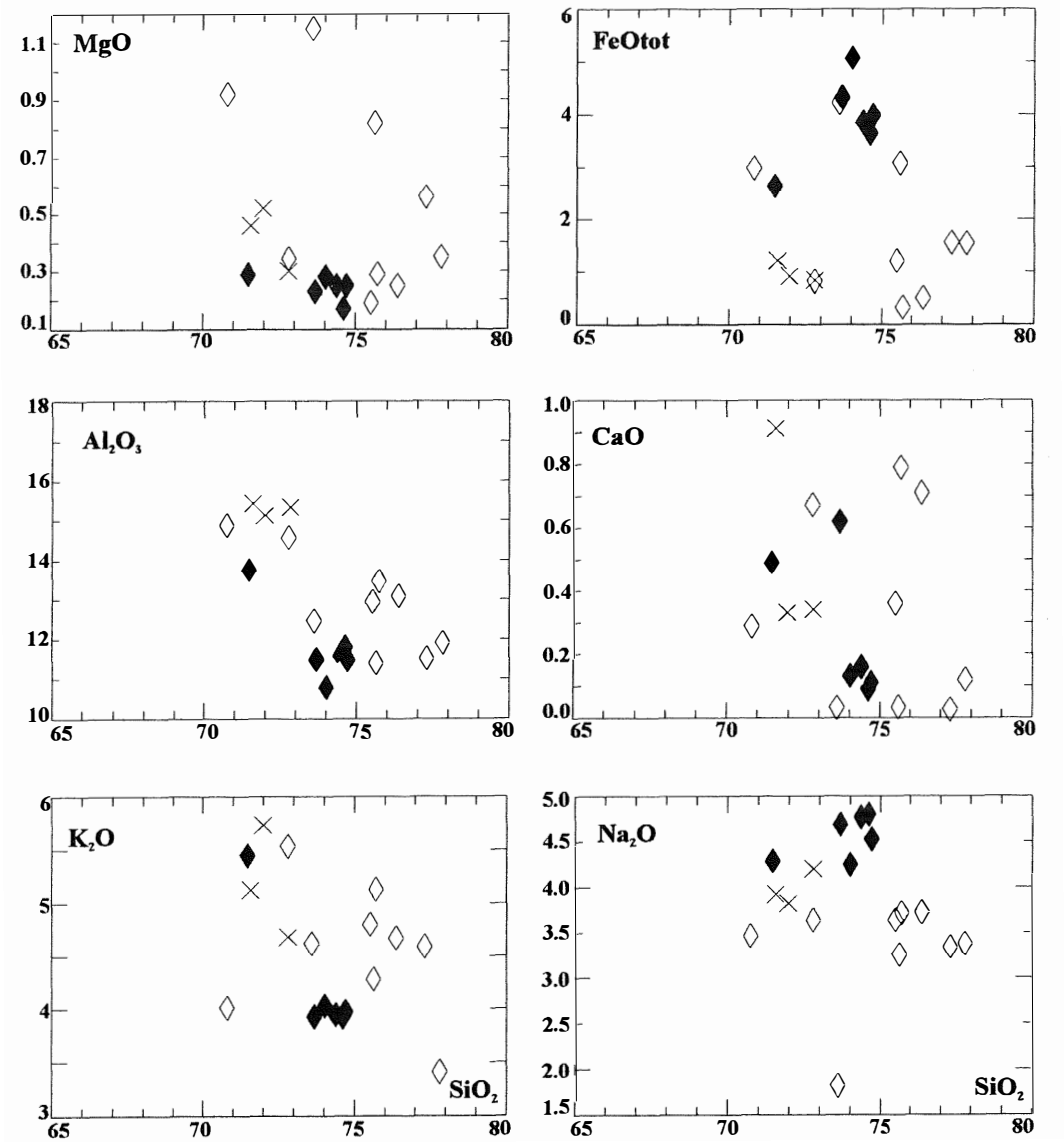

Fig. 18 - Selected major elements *vs.* SiO_2 diagrams for NW Corsica rhyolitic dyke rocks. Symbols as in fig. 3.

by their trends on the ORG-normalized spidergrams (fig. 20). These are strongly enriched in all elements from K to Yb and show a distinct negative Ba anomaly, controlled by alkali feldspar fractionation. The strong similarity shown in fig. 20 with the Evisa hypersolvus granite (source of data from Bonin *et al.,* 1978, Bonin, 1988) is further confirmation of the A-type character of PAR.

As regards REE patterns, PAR are the most enriched compared with the other rhyolitic dykes (ΣREE: 501÷1383 ppm, Table 10). On chondrite-normalized diagrams (fig. 15) they show very poorly fractionated trends (La_n/Yb_n=2.3÷3.4),

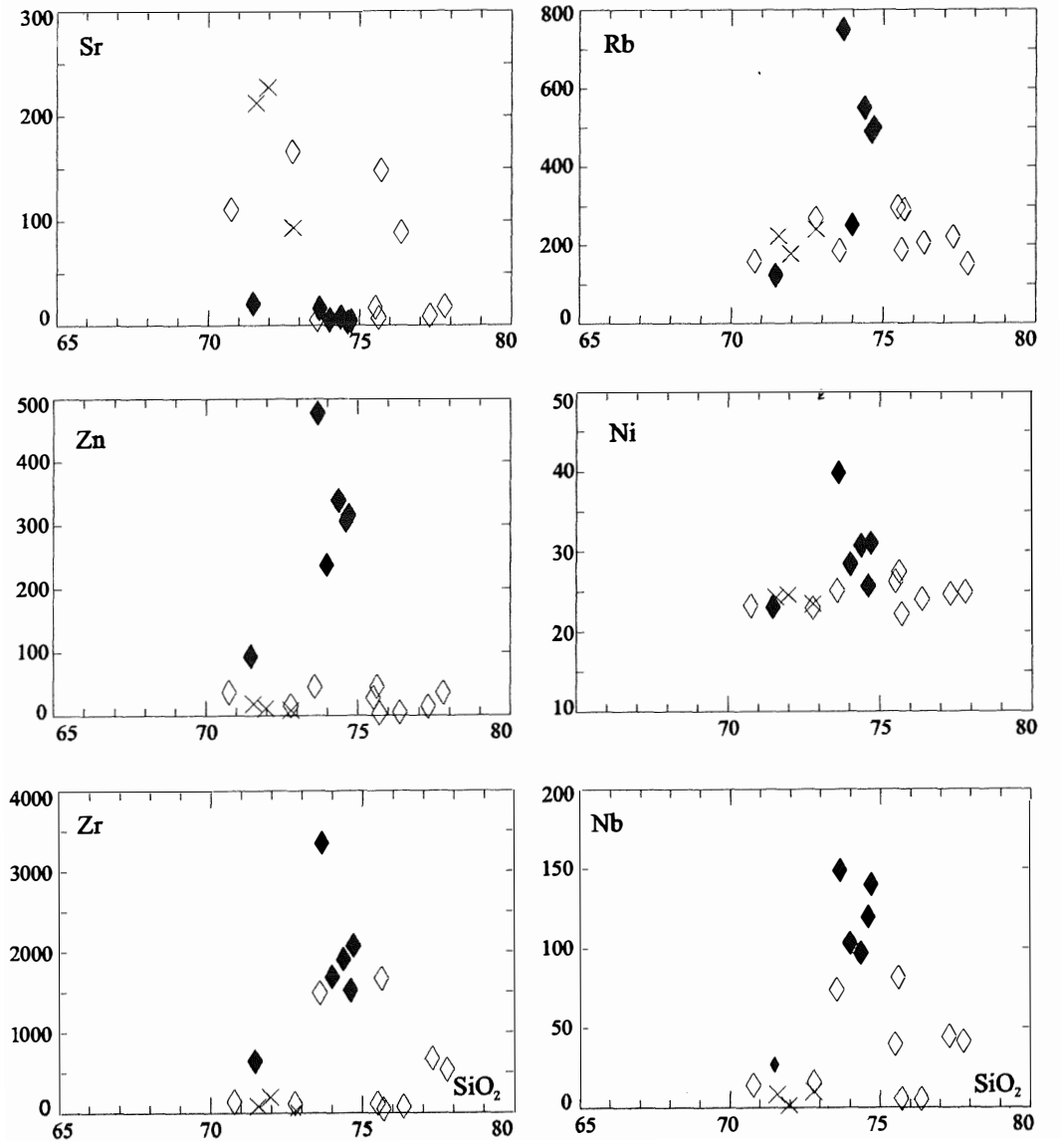

Fig. 19 - Selected trace elements *vs.* SiO_2 diagrams for NW Corsica rhyolitic dyke rocks. Symbols as in fig. 3.

except for lithotypes with ferroaugite clinopyroxene (La_n/Yb_n=12), whose higher fractionation degree is due a definite decrease in HREE. Strong negative Eu anomalies (Eu/Eu*: 0.11÷0.15, Table 10), also characteristic of A-type granites, are evident in fig. 15.

PR are the least evolved among rhyolitic dykes, SiO_2 contents being around 72%, and they show the highest contents of Al_2O_3 (around 15%), Sr (112÷212 ppm) and Ba (513÷608 ppm), typical of calc-alkaline granite. This affinity is confirmed by the trends

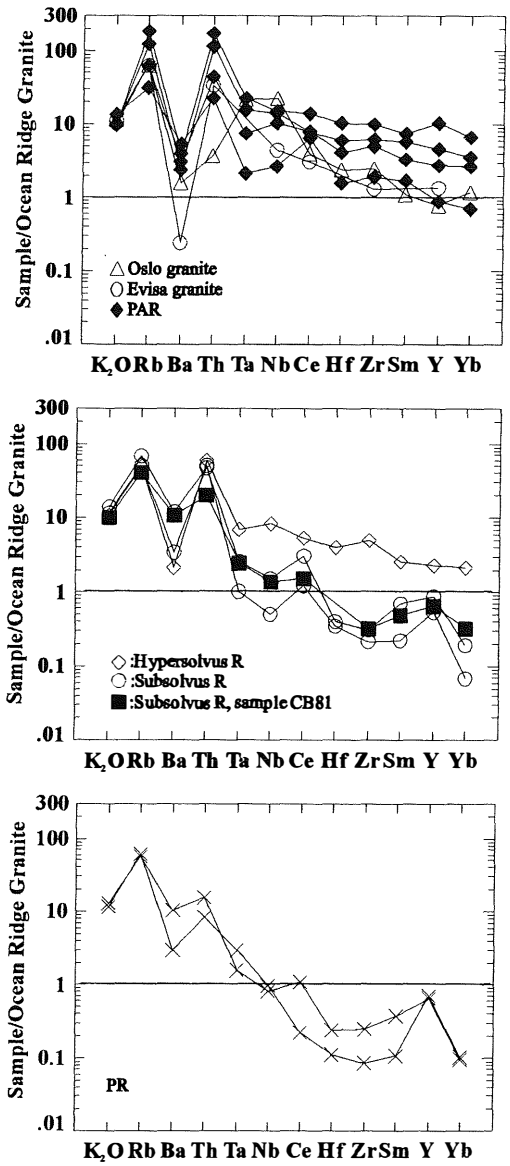

Fig. 20 - Ocean ridge granite (ORG) normalized spidergrams for some representative NW Corsica rhyolitic dykes. Normalizing values from Pearce *et al.* (1984). Abbreviations as in fig. 3.

displayed in fig. 20, characterized by low HFSE abundances, especially Hf and Zr (Th is transitional in this respect) and strong LILE enrichment. It is noteworthy how sample CB68 is particularly depleted in Hf, Zr, Ce and Sm, probably in response to fractionation of minor phases like zircon, apatite and allanite, which are found in the other PR. As regards REE distribution, PR are much less enriched (fig. 15, ΣREE: 21÷88 ppm) compared with the other rhyolitic dykes and show variable LREE/HREE fractionation (La_n/Yb_n=2.7÷16). They are characterized by low HREE contents (about 5 times chondritic values), explained by the presence of restitic HREE carrier phases, like garnet, in the source. They also show a less marked negative Eu anomaly (Eu/Eu*: 0.50÷0.87) compared with PAR and R, linked to the abundance of plagioclase and suggesting differences in the magma source. Sample CB68 has very low REE abundances (ΣREE: 21 ppm) and the least fractionated trend (La_n/Yb_n=2.7). Fractionation of minor phases such as allanite and monazite may account for its remarkably low LREE contents (10 times chondritic values). However, two other possible explanations may be either a higher degree of partial melting of a common protolith, or simply provenance of PR from different protoliths. In this regard, isotopic data are in progress.

R are represented by variably evolved rocks, SiO_2 being between 70% and 78%. Alkali contents range between 6.4% and 9.2%, the lower values mainly referring to Na_2O loss. In the major and trace element variation diagrams, two clearly separate groups are shown (figs. 18-19).

The first group, petrographically represented by R with discrete K and Na feldspars and therefore regarded as subsolvus, has higher CaO, Al_2O_3 and Sr contents than the second group, which is represented by granitic porphyries with alkali feldspar of intermediate composition and therefore regarded as hypersolvus; the latter displays negative trends in the MgO *vs.* SiO_2 and FeOt vs. SiO_2 diagrams, probably in response to biotite and/or amphibole fractionation. Fig. 20 shows that the hypersolvus R trends are broadly comparable with those of PAR, although less enriched. They also show extremely similar REE

distributions compared with PAR (fig. 15), having very high REE contents (ΣREE: 497), marked negative Eu anomalies (Eu/Eu*: 0.07) and low LREE/HREE fractionation degrees (La_n/Yb_n=2.8). Taking into account their extreme fractionation degree, most hypersolvus R may be considered as residual melts enriched in HFSE and REE.

As regards subsolvus R, their incompatible elements and REE distributions are almost the same as those of PR. In fig. 20, the main difference in the relative trends is represented by the slightly higher Th enrichment of subsolvus R, whereas in the chondrite-normalized diagram (fig. 15) subsolvus R show more marked LREE/HREE fractionation (La_n/Yb_n=21÷25), linked to a strongly HREE fractionated saddle-like trend showing evident impoverishment in the middle HREE, possibly due to titanite fractionation. An exception is sample CB81, whose lower degree of evolution (SiO_2=71) is responsible for the low LREE/HREE fractionation (La_n/Yb_n=6.4) and the less marked Ba negative anomaly (see figs. 15 and 20).

The above chemical and petrographic similarities between hypersolvus R and PAR on one hand and subsolvus R and PR on the other, allow us to infer a common magma source respectively for the first and second groups, and to relate them to different tectonic settings. Thus, based on trace elements and REE modeling, we refer PAR and hypersolvus R to A-type granites and use the Y/Nb parameter to constrain their genesis (Eby, 1990). This parameter, as well as Yb/Ta, is a good petrogenetic indicator, since it remains reasonably constant throughout the evolution of a particular suite over a large range of SiO_2 values. The distinction among different A-type granitoids follows this criterion. Granitoids with a value of Y/Nb<1.2 and generally low initial $^{87}Sr/^{86}Sr$ ratios are considered to be directly derived from an OIB-like mantle source, which may have undergone some crustal interaction. Granitoids with Y/Nb>1.2 and highly variable initial $^{87}Sr/^{86}Sr$ ratios reveal a more complex petrogenetic history, potentially having either an important mantle component in their genesis or being totally of crustal origin. PAR and hypersolvus R belong to the second group (see Table 10) and present both mantle and crustal characters. The mantle signature is highlighted in fig. 20 by the similarity with the Oslo granitoids, the low initial $^{87}Sr/^{86}Sr$ ratio values of which (0.7038-0.7041) refer to genesis by fractionation of a basaltic parent magma originating from an enriched mantle source (Neumann, 1980). However, Th higher contents for PAR and hypersolvus R point to crustal involvement in their genesis, whereas less marked Nb and Ta enrichment indicates depletion of their mantle source compared with the Oslo granitoids. The relation to an anorogenic setting for PAR and hypersolvus R is evident from the LogNb *vs.* LogY diagram (fig. 21, Pearce *et al.,* 1984), in which they plot in the within-plate granite (WPG) field; their similarity with the Upper Permian Evisa granite ascribes them to an incipient phase of rifting (Bonin and Platevoet, 1988). Instead, PR and subsolvus R plot in the volcanic arc and syn-collisional granite field (VAG+synCOLG) of fig. 21, in a geodynamic setting still related to an orogenic domain and

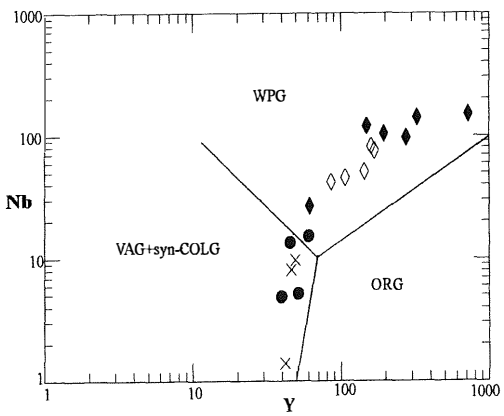

Fig. 21 - LogNb *vs.* logY tectonic discrimination diagram (after Pearce *et al.,* 1984) for NW Corsica rhyolitic dykes. WPG: within-plate granites; ORG: ocean ridge granites; VAG: volcanic arc granites; syn-COLG: syn-collisional granites. Symbols: solid diamonds: peralkaline rhyolite (PAR); empty diamonds: hypersolvus R; full circles: subsolvus R; *x:* peraluminous rhyolite (PR).

thus predating PAR and hypersolvus R emplacement.

CONCLUDING REMARKS

Post-batholithic dyke magmatism in NW Corsica is characterized by a large variety of products with essentially bimodal distribution (figs. 3, 4). The scarcity of intermediate compositions may be due to the relatively fast ascent and cooling of these magmas in transtensive conditions, which do not favour fractionation processes and mixing phenomena. Instead, the prevalence of granodioritic and monzogranitic lithotypes making up the Hercynian plutons of Corsica indicates that the magma remained at length in the crustal environment, with consequent slow cooling fractionation. Contamination processes (Brotzu *et al.,* 1993) or interaction with magmas of different compositions (Tommasini *et al.,* 1995) represent further supporting evidence in this regard.

The basic dykes are represented by two distinct phases, respectively with calc-alkaline and mildly alkaline affinity, the latter called basaltic due to the prevalence of dykes with basaltic composition. Calcic amphibole (edenite-magnesiohornblende) and andesine plagioclase in intergranular texture are the main minerals of the calc-alkaline dykes, ranging in composition from basaltic andesites to andesites (BA, A), whereas albitized plagioclase and titaniferous augite characterize basaltic dykes (AB, TrB, TchB, TchBA). The crystallization of kaersutite in AB also supports their alkaline character.

Of all the basic dykes, only one BA with no evidence of crystal cumulus may be considered the closest to a primitive liquidus (Mg*=65; Cr=420 ppm). An origin from lithospheric mantle, metasomatized in an orogenic to late-orogenic phase, has already been proposed for similar Sardinian and southern Corsica dyke rocks (Traversa *et al.*, 1997). Combined geochemical features, between subduction-related and intracontinental magmatism (figs. 13, 16), support this origin also for the NW Corsica calc-alkaline rocks. Mixing from other sources is more improbable, since corresponding petrographic and field evidence is lacking.

Mass balance calculations indicate evolution from AB to more evolved basaltic dykes TchBA by fractionation of a mineral assemblage consisting of olivine, augite and mainly labradorite plagioclase (Table 11). Trace elements and REE modeling for less evolved basalts (AB, TrB) lead us to infer for them generation by partial melting of subduction-modified lithospheric mantle, like that which gave rise to the calc-alkaline magmatism, but related to an already post-orogenic intracontinental domain (see fig. 16). The mildly alkaline basaltic dyke magmatism of NW Corsica may predate the incipient Upper Permian rifting regime, during which numerous acidic alkaline-peralkaline ring complexes emplaced in northern and central Corsica. Peralkaline rhyolitic dykes (PAR) and hypersolvus rhyolitic dykes with biotite (hypesolvus R), detected by us in the areas of Calasima, Calenzana and the Fango valley (see fig. 1), show petrographic and geochemical characters very similar to those of the Upper Permian peralkaline granites of the same area (cfr. Evisa hypersolvus granite in fig. 20), the main difference being the structural situation. Both are in fact considered as anorogenic, trace elements and REE distributions highlighting a strong affinity with A-type granites. The Sr_i ratio value of 0.7034±0.0011 found by Bonin *et al.* (1978) in peralkaline granites from the Evisa complex indicates a mantle signature, with possible crustal involvement (Eby, 1990) as also confirmed by Th enrichment (cfr. Oslo granitoid in fig. 20). Since there is no evidence of fractionation links between basic, mildly alkaline and peralkaline rhyolitic (PAR) magmas and since intermediate types are lacking, we consider the PAR as primary melts derived from an appropriate mantle source of basaltic composition.

Besides PAR and hypersolvus R, acidic dykes are represented by numerous subsolvus

rhyolitic dykes with biotite (subsolvus R) and subordinate peraluminous microgranite (PR) outcropping in the Balagne region (see fig. 1). On the basis of the same directions of intrusion and the calc-alkaline affinity, the latter may be considered very similar to the microgranite identified by Fumey-Humbert *et al.* (1986) in the same area and considered as possible feeder pipes of the Lower Permian calc-alkaline volcanism. However, preliminary $^{40}Ar/^{39}Ar$ geochronological data (Buraglini *et al.,* in progress) performed on some PR give an age around 320 Ma, which slightly postdates the host rock Mg-K calcalkaline association (322±12 Ma, Cocherie *et al.,* 1992). Therefore, on the basis of time relationships, this peraluminous microgranite may be considered as a probable anatectic melt connected to the Mg-K calcalkaline association, referred to a syn-late-orogenic geodynamic setting by Menot and Orsini (1990). Also in southern Sardinia (Sarrabus) peraluminous leucogranite dykes have been identified that are slightly younger (Rb-Sr ages on muscovite: 293-292 Ma, Ronca *et al*., 1999) than the granitic plutons they intrude (Capo Carbonara granodiorite, 301-298 Ma, Nicoletti *et al*., 1982 and references therein).

REE distributions for PR and subsolvus R (fig. 15) support variable degrees of partial melting and the presence of restitic HREE carrier phases, like garnet, in the crustal source. The more or less marked negative Eu anomaly (Eu/Eu*: 0.50÷0.87) shown by rocks of the same evolutive degree like PR (fig. 15) may indicate differences in the original protoliths. In this regard, Sr and Nd isotopic data for comparable peraluminous rhyolitic dykes from Sardinia highlighted two different protoliths: one more radiogenic (initial $^{87}Sr/^{86}Sr$=0.71490÷0.71731, $\varepsilon^{t}Nd$= –7.45) with a pelitic metasedimentary source, the other less radiogenic (initial $^{87}Sr/^{86}Sr$=0.70757÷0.71121, $\varepsilon^{t}Nd$= -5.7÷-6.3) with an intermediate meta-igneous source (Traversa and Vaccaro, 1992; Ronca *et al.,* 1999). Isotopic data for PR are being collected.

APPENDIX

Analytical procedures

Major oxides and trace elements of whole rocks were determined by X-ray fluorescence, except for FeO (wet chemical titration), MgO (atomic absorption spectrometry) and L.O.I. (standard gravimetric techniques). XRF analyses were carried out at the Institute of Earth Sciences, University of Catania, on a Philips PW1400 automatic spectrometer following the methods of Franzini and Leoni (1972) and Kaye (1965) for major and trace elements, respectively. REE, Hf and Ta were detected by the ICP-MS method (inductive coupled plasma-massa spectrometry) at the Activation Laboratories Ltd. of Ontario (Canada). Chemical compositions of mineral phases and major element analyses were carried out at the Department of Earth Sciences, University of Florence, on a JEOL JxA 8600 electron microprobe (wavelength dispersive mode; accelerating potential 15 kV; beam current 20 nA). Natural and synthetic oxides and silicates were used as standard materials. Data were processed according to Bence and Albee (1968).

ACKNOWLEDGMENTS

This work is part of a research program supported by the Italian MURST, CNR grants (to G. Traversa) and the «Centro di Studi per gli equilibri sperimentali in minerali e rocce» of the CNR. We are particularly grateful to Elisabetta Giuffrida and Mimmo La Rocca, Department of Earth Sciences, University of Catania, for their assistance in performing major and trace element analyses, Dr. Lino Cirrincione for his significant help in processing XRF data, and Dr. F. Olmi, Department of Earth Sciences, University of Florence, for microprobe analyses. We are also greatly indebted to P.Atzori and B.Bonin for their critical comments and helpful suggestions.

REFERENCES

AFIFI A.M. and ESSENE E.J. (1988) — *MINFILE, a microcomputer program for storage and manipulation of chemical data on minerals.* Am. Miner., **73**, 446-448.

ARTHAUD F. and MATTE Ph. (1976) — *Arguments géologiques en faveur de l'absence de mouvements relatifs de la Corse par rapport à la Sardaigne depuis l'orogenèse hercynienne.* C.R. Acad. Sc. Paris, **t. 283**, Série D.

ATZORI P. and TRAVERSA G. (1986) — *Post-granitic permo-triassic dyke magmatism in eastern Sardinia (Sarrabus p.p., Barbagia, Mandrolisai, Goceano, Baronie and Gallura).* Per. Mineral., **55**, 203-231.

BAKER B.H., GOLES G.G., LEEMAN W.P. and LINDSTROM M.M. (1977) — *Geochemistry and petrogenesis of a basalt-benmoreite-trachyte suite from the southern part of the Gregory Rift, Kenya.* Contrib. Mineral. Petrol., **64,** 303-332.

BALDELLI C., BIGAZZI G., ELTER F.M. and MACERA P. (1986) — *Description of a permo-trias alkaline lamprophyre embedded into the micaschists of garnet-staurolite-kyanite grade north-eastern Sardinia island.* Meeting «Paleozoic, stratigraphy, tectonics, metamorphism and magmatism in Italy», Siena, December 13-14, 1986.

BENCE A.E. and ALBEE A.L. (1968) — *Empirical correction factors for the electron microanalyses of silicates and oxides.* J. Geol., **76**, 382-483.

BONIN B., GRELOU-ORSINI C. and VIALETTE Y. (1978) — *Age, Origin and Evolution of the Anorogenic Complex of Evisa (Corsica): a K-Li-Rb-Sr Study.* Contrib. Mineral. Petrol., **65**, 425-432.

BONIN B. (1980) — *Le complexes acides alcalins continentaux: l'exemple de la Corse.* These d'Etat, Univ. Paris, IV, pp. 758.

BONIN B. (1988) — *Peralkaline granites in Corsica: some petrological and geochemical constraints.* Rend. Soc. It. Min. Petr., **43-2**, pp. 281-306.

BONIN B. and PLATEVOET B. (1988) — *Interactions fluide-solide et phénomènes de fénitisation dans le magmatisme alcaline Corse: l'exemple de l'association du Vieux Pont d'Ota.* Bull. Soc. Géol. Fr. **8,** IV, 571-578.

BOUGAULT H. and HEKINIAN R. (1974) — *Rift valley in the Atlantic Ocean near 36 degrees 50'N; petrology and geochemistry of basalt rocks.* Earth Planet. Sci. Lett., **24**, 249-261.

BOYNTON W.V. (1984) — *Cosmochemistry of the Rare Earth Elements: meteorite studies.* In: HENDERSON P. (ed.). «Rare Earth Element Geochemistry». Elsevier, 63-114.

BRALIA A., GHEZZO C., GUASPARRI G. and SABATINI G. (1981) — *Alcuni aspetti genetici del batolite ercinico sardo.* Rend. Soc. It. Miner. Petr., **37**, 701-764.

BROTZU P., CALLEGARI E. and SECCHI A. (1993) — *The search for the parental magma of the high-K calcalkaline igneous rock series in the southernmost Sardinia Batholith.* Per. Mineral., **62**, 253-280.

BRUNETON P., BRISSET F., COCHEME J.J., ORSINI J., VELLUTINI P. and VINCENT P.M. (1976) — *Presence d'une structure annulaire en Gallura (Sardaigne septentrionale).* Compt. Rend. Hebd. des Seances de l'Ac. des Sci., Serie D: Sciences Naturelles, **282**, 24, 2127-2130.

BURAGLINI N., RENNE P. and TRAVERSA G. — *$^{40}Ar/^{39}Ar$ geochronological data on late-Hercynian dykes from NW-Corsica (France).* (In progress).

CABANIS B. and LECOLLE M. (1989) — *Le diagramme La/10-Y/15-Nb/8: un outil pour la discrimination des séries volcaniques et la mise en évidence des processus de mélange et/ou de contamination crustale.* C.R. Acad. Sci., Ser.II, **309**, 2023-2029.

CABANIS B., COCHEMÉ J.J., VELLUTINI P.J., JORON J.L. and TREUIL M. (1990) — *Post-collisional Permian volcanism in northwestern Corsica: an assessment based on mineralogy and trace-element geochemistry.* J.Volc. Geotherm. Res., **44**, 51-67.

CARMIGNANI L. and ROSSI Ph. (2000) — *Carta geologica e strutturale della Sardegna e della Corsica (1:500.000).* CARMIGNANI L. and ROSSI Ph., Coordinators. Servizio Geologico d'Italia and BRGM-Service Géologique National.

CAROSI R., GANDIN A., GATTIGLIO M. and MUSUMECI G. (1992) — *Geologia della Catena Ercinica in Sardegna-Zona Esterna.* In: CARMIGNANI L., PERTUSATI P.C., BARCA S., CAROSI R., DI PISA A., GATTIGLIO M., MUSUMECI G. & OGGIANO G. (Eds.). «Geologia della Catena Ercinica in Sardegna. Guida alla Escursione sul basamento paleozoico della Sardegna». Gruppo Informale di Geologia Strutturale, 43-75.

CASTORINA F. and PETRINI R. (1989) — *Radiometric geochronology: some constraints to the isochron method by an iterative least-squares approach.* Geochem. J., **23**, 101-109.

COCHERIE A., GUERROT C. and ROSSI Ph. (1992) — *Single-zircon dating by step-wise Pb evaporation: comparison with other geochronological techniques applied to the Hercynian granites of Corsica, France.* Chem. Geol., **101,** 131-141.

COCHIERE A., ROSSI Ph., FOUILLAC A.M. and VIDAL Ph. (1994) — *Crust and mantle contribution to granite genesis. An example from the Variscan batholith of Corsica, France, studied by trace-element and Nd-Sr-O isotope systematics.* Chem. Geol., **115**, 173-211.

COCOZZA T., CONTI L., COZZUPOLI D., LOMBARDI G., SCHARBERT S. and TRAVERSA G. (1977) — *Rb/Sr age and geo-petrologic evolution of crystalline rocks in southern Sulcis (Sardinia).* N. Jb. Geol. Paläont. Mh., **2**, 95-102.

DE LA ROCHE H., LETERRIER, P., GRANDCLAUDE P. and MARCHAL M. (1980) — *A classification of volcanic and plutonic rocks using R1R2-diagram and major element analyses. Its relationships with current nomenclature.* Chem. Geol., **29**, 183-210.

DEBON F. and ZIMMERMANN J.L. (1993) — *Mafic dykes from some plutons of the western Pyrenean Axial Zone (France, Spain): markers of the transition from late-Hercynian to early-Alpine events.* Schweiz. Mineral. Petrogr. Mitt., **73**, 421-433.

DEL MORO A., DI SIMPLICIO P., GHEZZO C., GUASPARRI G., RITA F. and SABATINI G. (1975) — *Radiometric data and intrusive sequence in the Sardinian Batholith.* N. Jb. Miner. Abh., **126/1**, 28-44.

DEL MORO A., DI PISA A. and OGGIANO G. (1996) — *Relationship between an autunian volcano-sedimentary succession and the Tempio Massif granites (northern Sardinia). Geochronology and field constraints.* Plinius, **16**, 94-95.

DYMEK R.F. (1983) — *Titanium, aluminum and interlayer cation substitutions in biotite from high-grade gneisses, West Greenland.* Am. Miner., **68**, 880-899.

EBY G.N. (1990) — *The A-type granitoids: a review of their occurrence and chemical characteristics and speculations on their petrogenesis.* Lithos, **26**, 115-134.

EDEL J.B., MONTIGNY R. and THUIZART R. (1981) — *Late Paleozoic rotations of Corsica and Sardinia: new evidence from paleomagnetic and K-Ar studies.* Tectonophysics, **79**, 201-223.

EGEBERG, A.T., BONIN B. and SARENSEN H. (1993) — *The Bonifatto peralkaline granites (NW Corsica): a possible case of evolution through volatile transfer.* Bull. Soc. Géol. France, t. **164**, n° 5, pp. 739-758.

FINGER L.W. (1972) — *The uncertainty in the calculated ferric iron content of a microprobe analysis.* Carnegie Institution of Washington, **71**, 600-603.

FONTANA G., GELMINI R. and LOMBARDI G. (1982) — *Le successioni sedimentarie e vulcaniche carbonifere e permo-triassiche della Sardegna.* In: CARMIGNANI L., COCOZZA T., GHEZZO C., PERTUSATI P. e RICCI C.A. (Eds.), Guida alla Geologia del Paleozoico sardo. Guide Geologiche Regionali. Soc. Geol. It., 183-192.

FRANZINI M. and LEONI L. (1972) — *A full matrics correction in X-ray fluorescence analysis of rock samples.* Atti Soc. Tosc. Sc. Nat., Pisa, Mem. 79 (Serie A), 7-22.

FUMEY-HUMBERT F., MÉNOT R.P. and ORSINI J.B. (1986) — *Mise en évidence d'un magmatisme filonien original, d'âge permien inférieur, en Balagne (Corse du Nord-Ouest).* C.R. Acad. Sc. Paris, **t. 303**, Série II, n°12.

GALLEGHER K. and HAWKESWORTH C.J. (1992) — *Dehydration melting and the generation of continental flood basalts.* Nature, **358**, 57-59.

GHEZZO C. and ORSINI J.B. (1982) — *Lineamenti strutturali e composizionali del batolite ercinico sardo-corso in Sardegna.* In: CARMIGNANI L., COCOZZA T., GHEZZO C., PERTUSATI P. E RICCI C.A. (Eds.). «Guida alla Geologia del Paleozoico sardo. Guide Geologiche Regionali». Soc. Geol. It., 165-181.

HAWKERSWORTH C.J., GALLAGHER K., HERGT J.M. and MCDERMOTT F. (1993) — *Trace element fractionation processes in the generation of island arc basalts.* In: COX K.G., MCKENZIE D.P., WHITE R.S. (Eds.), «Melting and Melt Movement in the Earth.». Phil. Trans. R. Soc. London, Oxford University Press, A342, pp. 179-191.

HAWTHORNE F.C. (1982) — *Crystal chemistry of the amphiboles.* In: VEBLEN D.R. (ed.). «Amphiboles and other hydrous pyriboles – Mineralogy». Reviews in Mineralogy, **9A,** 1-102.

HUERTAS M.J. and VILLASECA C. (1994) — *The last post-Variscan magmatic activity in the Spanish Central System: calc-alkaline dyke swarm.* Schweiz. Mineral. Petrogr. Mitt., **74**, 383-401.

IRVINE T.N. and BARAGAR W.R.A. (1971) — *A guide to the chemical classification of the common volcanic rocks.* Can. J. Earth Sci., **8**, 523-548.

KAYE M.J. (1965) — *X-ray fluorescence determination of several trace element in some standard geochemical samples.* Geochim. Cosmochim. Acta, **29**, 139-142.

LE MAITRE R.W. (Ed.) (1989) — *A classification of igneous rocks and glossary of terms.* Blackwell Scientific Publications, pp.193.

LE ROEX A.P. and EERLANK A.J. (1982) — *Quantitative evaluation of fractional crystallization in Bouvet Island lavas.* J. Volc. Geotherm. Res., **13**, 309-338.

LEAKE B.E., WOOLLEY A.R., ARPS C.E.S., BIRCH W.D., GILBERT M.C., GRICE J.D., HAWTHORNE F.C., KATO A., KISCH H.J., KRIVOVICHEV V.G., LINTHOUT K., LAIRD J., MANDARINO J., MARESCH W.V., NICKEL E.H. and ROCK N.M.S. (1997) — *Nomenclature of amphiboles. Report of the Subcommitee on Amphiboles of the International Mineralogical Association Commission on New Minerals and Mineral Names.* Eur. J. Mineral., **9**, 623-651.

LEMARCHAND F., VILLEMANT B. and CALAS G. (1987) — *Trace elements distribution coefficients in alkaline series.* Geochim. Cosmochim. Acta, **51**, 1071-1081.

LETERRIER J., MAURY R.C., THONON P., GIRARD D. and MARCHAL M. (1982) — *Clinopyroxene composition as a method of identification of the magmatic affinities of paleo-volcanic series.* Earth Planet. Sci. Lett., **59,** 139-154.

LOMBARDI G., COZZUPOLI D. and NICOLETTI M.

(1974) — *Notizie geopetrografiche e dati sulla cronologia K-Ar del vulcanismo tardopaleozoico sardo.* Per. Mineral., **43**, 221-312.

MACERA P., CONTICELLI S., DEL MORO A., DI PISA A., OGGIANO G. and SQUADRONE A. (1989) — *Geochemistry and Rb-Sr age of syn-tectonic peraluminous granites of Western Gallura, Northern Sardinia: constraints on their genesis.* Per. Mineral., **58**, 25-43.

MALUSKI H. and LANCELOT J.R. (1976) — *Age permien des granites alcalins de Corse par les méthodes $^{40}Ar/^{39}Ar$ et U/Pb.* Réunion Ann. Sci. de la Terre, Paris, 278.

MALUSKI H. (1974) — *Mise en évidence par la méthode $^{40}K/^{40}Ar$ de l'âge permien de certains granites hyperalcalins de Corse.* C. R. Somm. Soc. Géol. Fr. 93-95.

MALUSKI H. (1976) — *$^{40}Ar/^{39}Ar$ ages of biotites from Corsica and arguments for Permian age of alkaline granitic intrusion.* Contrib. Mineral. Petrol., **58**, 305-317.

MANIAR P.D. and PICCOLI P.M. (1989) — *Tectonic discrimination of granitoids.* Geol. Soc. Am. Bull., **101,** 635-643.

MARRE J. and ROSSI Ph. (1981) — *Architecture d'un secteur du batholite corso-sarde: le régions d'Ajaccio et Sartène.* Bull. B.R.G.M., **2**, I, 2, 153-167.

MENOT R.P. and ORSINI J.B. (1990) — *Evolution du socle anté-stéphanien de Corse: événements magmatiques et métamorphiques.* Schweiz. Mineral. Petrogr. Mitt., **70**, 35-53.

MORIMOTO N. (1988) — *Nomenclature of pyroxenes.* Mineralogical Magazine, **52**, 535-550.

NEUMANN E.R. (1980) — *Petrogenesis of the Oslo Region Larvikities and Associated Rocks.* J. Petrol., **21**, part.3, 499-531.

NICOLETTI M., ARDANESE L.R. and COLASANTE S. (1982) — *La granodiorite di Capo Carbonara (Sardegna, Italia). Età K-Ar di fasi minerali in paragenesi.* Rend. Soc. It. Min. Petr., **38,** 765-769.

ORSINI J.B. (1980) — *Le batholite corso-sarde: anatomie d'un batholite hercynien. Composition, structure, organisation d'ensemble. Sa place dans la chaine Varisque francaise.* Ph.D. Thesis, Université de Aix-Marseille III, 390pp.

OTTAVIANI M.M., TURPAULT M.P. and MEUNIER A. (1989) — *Typologie des altération hydrithermales dans le socle hercynien: une phase hydrothermale de l'Alpin en Corse hercynienne (France).* C.R. Acad. Sci. Paris. Sér.II: Sci. Terre, **309**, 1317-1323.

PANI E., RIZZO R. and RAUDSEPP M. (1997) — *Manganoan-fayalite-bearing granitic pegmatite from Quirra, Sardinia: relation to host plutonic rocks and tectonic affiliation.* Canad. Mineral., **35**, 119-133.

PAPIKE J.J., CAMERON K. and BALDWIN K. (1974) — *Amphibole and pyroxenes: characterization of other than quadrilater components and estimates of ferric iron from microprobe data.* Bull. Geol. Soc. Amer., **6**, 1053-1054.

PASQUALI C. and TRAVERSA G. (1996) — *Petrography and Mineral Chemistry of late-Hercynian dykes from southern Corsica.* Per. Mineral., **65**, 213-256.

PASQUALI C. (1998) — *Petrologia del magmatismo filoniano tardo-ercinico della Corsica meridionale.* Tesi di Dottorato, Università degli Studi di Perugia.

PEARCE J.A. (1982) – *Trace element characteristics of lavas from destructive plate boundaries.* In: THORPE R.S. (Ed.), «Andesites», John Wiley & Sons.

PEARCE J.A., HARRIS N.B.W. and TINDLE A.G. (1984) — *Trace element dicrimination diagrams for the tectonic interpretation of granitic rocks.* J. Petrol., **25**, Part. 4, pp. 956-983.

PLATEVOET B. and BONIN B. (1991) — *Enclaves and mafic-felsic associations in the Permian alkaline province of Corsica, France; physical and chemical interactions between coeval magmas.* In: DIDIER J. and BARBARIN B. (Eds.), «Developments in Petrology», Elsevier, pp.191-204.

POITRASSON F., PAQUETTE J.L., MONTEL J.M., PIN C. and DUTHOU J.L. (1998) — *Importance of late-magmatic and hydrotermal fluids on the Sm-Nd isotope mineral systematics of hypersolvus granites.* Chem. Geol., **146**, 187-203.

POLI G., GHEZZO C. and CONTICELLI S. (1989) — *Geochemistry of granitic rocks from the Hercynian Sardinia-Corsica batholith: implication for magma genesis.* Lithos, **23**, 247-266.

POLI S. and SCHMIDT M.W. (1995) — *H_2O transport and release in subduction zones: experimental constraints on basaltic and andesitic systems.* J. Geophys. Res., **100,** 22299-22314.

QUIN J.P. (1968) — *Les granites alcalins et hyperalcalins du Nord-Ouest de la Corse.* Doct. Etat ès-Sci. Thesis, Univ. Marseilles, pp. 540.

RONCA S. and TRAVERSA G. (1996) — *Late Hercynian dyke magmatism of Sarrabus (SE Sardinia).* Per. Mineral., **65**, 35-70.

RONCA S., DEL MORO A. and TRAVERSA G. (1999) — *Geochronology, Sr-Nd isotope geochemistry and petrology of late-Hercynian dyke magmatism from Sarrabus (SE Sardinia).* Per. Mineral., **68**, 231-260.

ROSSI P. (1986) — *Organisation et genèse d'un grand batholite orogénique: le batholite calco-alcalin de la Corse.* Thèse Doct. Sc., Univ. Toulouse, Doc. BRGM, **107**, 292 p.

ROSSI Ph. and COCHERIE A. (1991) — *Genesis of a*

Variscan batholith: field, petrological and mineralogical evidence from the Corsica-Sardinia batholith. Tectonophysics, **195**: 319-346.

ROSSI Ph., DURAND-DELGA M. and COCHERIE A. (1993) — *Caractère volcano-plutonique du magmatisme calco-alcalin composite d'âge Stéphanien supérieur – Permien inférieur en Corse.* Principaux Résultats Scientifiques et Techniques du BRGM.

SCHUMACHER J.C. (1997) — *The estimation of ferric iron in electron microprobe analysis of amphiboles.* Appendix 2 of: LEAKE B.E., WOOLLEY A.R., ARPS C.E.S., BIRCH W.D., GILBERT M.C., GRICE J.D., HAWTHORNE F.C., KATO A., KISCH H.J., KRIVOVICHEV V.G., LINTHOUT K., LAIRD J., MANDARINO J., MARESCH W.V., NICKEL E.H. and ROCK N.M.S. (1997) – *Nomenclature of amphiboles. Report of the Subcommitee on Amphiboles of the International Mineralogical Association Commission on New Minerals and Mineral Names.* Eur. J. Mineral., **9**, 623-651.

SECCHI F.A., BROTZU P. and CALLEGARI E. (1991) — *The Arburese igneous complex (SW Sardinia, Italy). An example of dominant igneous fractionation leading to peraluminous cordierite-bearing leucogranites as residual melts.* Chem. Geol., **92,** 213-249.

SIMEI S. (1999) — *Petrografia del magmatismo filoniano tardo Ercinico di un settore della Corsica centro-settentrionale.* Tesi di Laurea in Petrografia, Relatore G. Traversa, Università degli Studi di Roma «La Sapienza», Roma.

STORMER JR. and NICHOLLS JC. (1978) — *XLFRAC a programme for interactive testing of magmatic differentiation model.* Comp. Geosci., **4**, 143-159.

SUN S.S. and MCDONOUGH W.F. (1989) – *Chemical and isotopic systematics of oceanic basalts: implication for mantle composition and processes.* In: SAUNDERS A.D. and NORRY M.S. (Eds.). «Magmatism in the Ocean Basins». Geol. Soc. Lond. Spec. Publ., 331-345.

TELLINGEN H.W. VAN, VERSCHURE R.H. and ANDRIESSEN P.A.M. (1996) — *Indications for an early Miocene mafic dike swarm in western Corsica. A combined fission track, isotopic and geochemical investigation.* Proc. Kon. Ned. Akad. v. Wetensch., **99** (1-2), 85-104.

TOMMASINI S. and POLI G. (1992) — *Petrology of late-Carboniferous Punta Falcone gabbroic complex, northern Sardinia, Italy.* Contrib. Mineral. Petrol., **110**, 16-32.

TOMMASSINI S., POLI G. and HALLIDAY A. (1995) — *The role of sediment subduction and crustal growth in Hercynian plutonism: isotopic and trace element evidence from the Sardinia-Corsica batholith.* J. Petrol., **36,** 5, 1305-1332.

TRAVERSA G. (1968) — *Ipoabissaliti melanocrate nelle facies ignimbritiche del Monte Tundoni (Sardegna settentrionale).* Per. Mineral., **37** (3), 1059-1082.

TRAVERSA G. (1969) — *Sulla giacitura ed età di alcuni filoni basici nelle vulcaniti ignimbritiche permiane della Gallura (Sardegna settentrionale).* Rend. Soc. It. Min. Petr. **25**, 149-155.

TRAVERSA G. (1979) — *Permian volcanism in Sardinia.* In: SASSI F.P. (ed.), I.G.C.P. N.5, Newsletter, **Vol. 1**, 127-140.

TRAVERSA G. and VACCARO C. (1992) — *REE distribution in the late hercynian dykes from Sardinia.* In: CARMIGNANI L. and SASSI F.P. (Eds.), IGCP n. 276, Newsletter, **Vol. 5**, Siena 1992, 215-226.

TRAVERSA G., RONCA S. and PASQUALI C. (1997) — *Post-hercynian basic dyke magmatism of the Concas-Alà dei Sardi alignment (Northern Sardinia-Italy).* Per. Mineral., **66**, 233-262.

VACCARO, C., ATZORI P., DEL MORO A., ODDONE M., TRAVERSA G. and VILLA I.M. (1991) — *Geochronology and Sr isotope geochemistry of late-hercynian dykes from Sardinia.* Schweiz. Mineral. Petrogr. Mitt., **71**, 221-230.

VELLUTINI P. (1977) — *Le magmatisme permien du Nord-Ouest de la Corse. Son extension en Méditerranée Occidentale.* Doct. Etat ès-Sci. Thesis, Univ. Marseille, p.276.

VIGLIOTTI L., ALVAREZ W. and MCWILLIAMS M. (1990) — *No relative rotation detected between Corsica and Sardinia.* Earth. Planet. Sci. Lett., **98**, 313-318.

VIGLIOTTI L. and LANGENHEIM V.E. (1995) — *When did Sardinia stop rotating? New paleomagnetic results.* Terra Nova, **7,** 424-435.

VILLEMANT B., JAFFREZIC H., JORON J.L. and TREUIL M. (1981) — *Distribution coefficients of major and trace elements: fractional crystallization in the alkali basalt series of Chaîne des Puys (Massif Central, France).* Geochim. Cosmochim. Acta, **45**, 1997-2016.

WESTPHAL M., ORSINI J. and VELLUTINI P. (1976) — *Le microcontinent corso-sarde, sa position initiale: données paléomagnétiques et raccords géologiques.* Tectonophysics, **30**, 141-157.

WHALEN J.B., CURRIE K.L. and CHAPPELL B.W. (1987) — *A-type granites: geochemical characteristics, discrimination and petrogenesis.* Contrib. Mineral. Petrol., **95**, 407-419.